



Sudan University of Science & Technology



College of Graduate Studies

**A Study on the Structure, Morphology and Optical Properties
of ZnO Nanostructures Films Synthesized using Different
Concentrations of Zinc Acetate**

دراسة التركيب و الهيئة و الخواص الضوئية لاغشية اكسيد الزنك النانوية
المحضرة باستخدام تراكيز مختلفة لخلات الزنك

**A thesis Submitted in Fulfillment of the Requirements
for the Degree of Doctor of Philosophy in Physics**

By:

Awatif Abas Bashir Abas

Supervisor

Prof. Mubarak Dirar Abd-Alla Yagoub

2021

Dedication

**This thesis is dedicated to my husband, my parents and my daughters
for their endless love, support and encouragement.**

Acknowledgment

It is my duty to acknowledge my heartfelt gratitude to my supervisor, Prof. Mubark Dirar, College of Science, Sudan University of Science and Technology, who has been a pillar support in stimulating and guiding me in all stages of this work. I'm indebted to him for imparting his wide experiences and knowledge in the field of nanoscience.

I also like to acknowledge the help provided by the technical staff in Faculty of Science at Al Neelain University, Sudan, for their logistic aids.

I also appreciate all the support I received from the Faculty of Engineering Gadarif University.

My appreciation also goes out to my husband for his encouragement and support all through my studies.

Abstract

Researchers are usually looking for simple methods like sol-gel process that leads to possible low cost and pure products and easy film processing on a variety of substrates for synthesizing metal oxides like ZnO nanostructures. The main aim of this study is to investigate the effect of different concentrations of zinc acetate on the structural, morphological and optical properties of Zinc oxide films nanostructures. The different concentrations of zinc acetate are 0.1, 0.2, 0.3, 0.4, 0.5, 0.6, 0.7, 0.8, 0.9 and 1.0 Moles respectively. The sol-gel method has been used as main step and then using coating technique deposited on ITO glass substrates to synthesize ZnO₂ nanostructure. The structural and the surface morphologies of as-synthesized ZnO materials were characterized by X-ray Diffraction, Fourier Transformer Infrared (FTIR) and Scanning Electron Microscopy (SEM). The XRD patterns for the ten samples of as-synthesized established that there is a sharp peak at $2\theta = 33.5027^\circ$ corresponding to (111) plane. Interestingly, among the ten samples, only sample ZnO 1.0 M explained the highest intensity of 9950 (a.u) for the sharp peak, which indicated that good crystallinity of the as-synthesized ZnO films samples increase with increasing the concentrations of zinc acetate. The crystal structure of as-synthesized ZnO produced local cubic structure that differed from the majority recent publishing papers which reported the most common for ZnO structure is hexagonal wurtzite. The FTIR resulted that the mean band for the ten samples around 1340 cm^{-1} is associated with the O-H bending vibration also the location of the absorption bands at the positions around 3640 cm^{-1} and 3910 cm^{-1} , is due to the stretching mode of H-O-H bending vibration of free charge or absorbed water which implies that the hydroxyl groups are retained in ZnO for different concentrations of zinc acetate. The surface morphologies of as-synthesized ZnO film structures have been investigated by Scanning Electron Microscopy (SEM). The SEM images for some samples revealed that the synthesized ZnO films formed like-date nanostructures with smooth surface. Also the results from SEM micrograph established that the size of the like-date nanostructures for sample 1.0 M equal to 11.77 nm where as for sample 0.1 M is equal to 148.38 nm. These results indicated that by increasing the zinc acetate concentrations lead to decreasing the size of nanostructures of as-synthesized ZnO

films. The results verified that the nanosizes received from SEM images agree with that calculated from XRD data except samples 1.0 and 0.9 moles. The optical properties; including absorption coefficient, refractive index, extinction coefficient, energy bandgap, real dielectric constant, imaginary dielectric constant and, optical and electrical conductivity were investigated by means of absorption, transmittance and reflectance spectra. The results indicated that the maximum value of the absorption coefficient α is $4.63 \times 10^3 \text{ cm}^{-1}$ materialized in the U.V region at the peak of wavelength 270 nm corresponding the concentration of 1.0 mole of zinc acetate where ever α at same wavelength decrease to $1.34 \times 10^3 \text{ cm}^{-1}$ for low concentration of 0.1 mole of zinc acetate. The refractive index (n) of the as-synthesized ZnO nanostructures represented a maximum peak at $n = 2.159$, except samples 0.2 mole and 0.1 M illustrated refractive index of values 2.128 and 2.044 respectively. This result in a good agreement with standard refractive index $n = 2.004$. Also the result demonstrated that the value of (n) begins to decrease between the wavelengths 306 - 344 nm at the region of the spectrum. This behavior may due to the nature of the sharp absorption of Zinc Oxide nanostructures that lead to an electronic transmission at the absorption edge. Concerning the energy bandgap, the results indicated that the as-obtained ZnO film nanostructures exhibited the highest bandgap of 3.889 eV for sample 0.1 molar, where as for sample 1.0 molar it exhibited the lowest value of 3.443 eV, which believed to possess a better conductivity. As a result, the bandgap energy received in this study decreases with increasing the concentration of the zinc acetate dehydrate. In addition, the study established that high magnitude of optical conductivity is found to be $1.34 \times 10^{11} \text{ sec}^{-1}$ for samples 1.0 M, 0.9 M, 0.8 M and 0.7 M respectively of as-prepared ZnO nanostructures which confirms the presence of very high photo-response. Although, samples 0.1 M, 0.2 M, 0.3 M, 0.4 M, 0.5 M and 0.6 M sharing same broad peak at wavelength of 268 nm, but are represented different optical conductivities 7.48×10^{10} , 9.01×10^{10} , 1.04×10^{11} , 1.17×10^{11} , 1.258×10^{11} and $1.309 \times 10^{11} \text{ sec}^{-1}$ respectively. The study confirmed that the electrical conductivity increases with increasing the concentrations of zinc acetate and that means the high concentration could account as an optimal condition for large electrical conductivity.

المستخلص

كثير من الباحثين يلجأون الي استخدام بعض الطرق البسيطة مثل طريقة تكوين الجل التي تؤدي الي انتاج مركبات نانوية منخفضة التكلفة. طريقة الجل أثارت إهتمام عدد كبير من الباحثين في تصنيع وتأليف المواد النانوية منها حبيبات اكسيد الزنك النانوية. الهدف الرئيس هو دراسة أثر التراكيز المختلفة لمركب اسيتيت الزنك علي شكل التركيب البلوري؛ الشكل السطحي و الخصائص الضوئية لمركب اكسيد الزنك النانوي. التراكيز المختلفة لاسيتيت الزنك علي النحو التالي 1.0، 0.9، 0.8، 0.7، 0.6، 0.5، 0.4، 0.3، 0.2، 0.1 مول. تم استخدام طريقة تكوين الجل كخطوة أولي مع استخدام تقنية الطلاء علي ركائز زجاجية. تمت دراسة الخصائص التركيبية و الشكل السطحي باستخدام تقنية حيود الأشعة السينية وجهاز المسح الإلكتروني علي التوالي. بينت الدراسة أن كل العينات العشر لمركب اوكسيد الزنك ذات تركيب بلوري مكعبي بسيط وكلها تشترك في ذروة حادة بمستوي تفضيلي (1 1) عند الزاوية $2\theta = 33.5027^\circ$. وجد من خلال نمط الأشعة السينية أن العينة ذات التركيز الكبير 1.0 مول لها اعلي شدة 9950 a.u وهذا دليل أن زيادة تركيز محلول اسيتيت الزنك ينتج عنه حالة تبلور جيدة لعينة مركب اوكسيد الزنك النانوي. ايضا استخدمت الدراسة تقنية تحويل فوريرير للطيف بالأشعة تحت الحمراء ووضحت النتائج ان النطاق الاساسي لكل عينات الدراسة العشرة يساوي 1340 cm^{-1} الذي يرتبط بالرابعة الاهتزازية O-H. كذلك بينت الدراسة أن رابطة الامتصاص عند النطاق 3640 cm^{-1} و النطاق 3910 cm^{-1} يرجعا الي الإستطالة الإهتزازية H-O-H التي توضح ان مجموعة الهيدروكسل عند إمتصاص الماء تعود الي تشكيل مركب اوكسيد الزنك لمختلف التراكيز نتيجة التغير في طول الرابطة. استخدمت الدراسة تقنية جهاز المسح الإلكتروني لتحليل ودراسة الشكل النانوي لكل العينات العشر. أوضحت الدراسة أن معظم العينات لاوكسيد الزنك تتألف من حبيبات نانوية شبيهة لأشكال بلحية. أيضا أثبتت الدراسة ان العينة 1.0 مول تتألف من حبيبات بلحية بأحجام 11.77 nm بينما العينة 0.1 مول تتألف من حبيبات بأحجام 148.38 nm وهذا يعني أن مع زيادة التراكيز تقل أحجام الحبيبات لمركب أوكسيد الزنك النانوي. اشارت الدراسة الي ان كل أحجام الجسيمات لأوكسيد الزنك التي قيست بجهاز المسح الإلكتروني تتفق مع الأحجام لذات الجسيمات النانوية التي قيست بجهاز حيود الأشعة السينية عدا العينتان 1.0 و 0.9 مول. لدراسة الخصائص الضوئية استخدمت الدراسة تقنية جهاز الأشعة فوق البنفسجية لتحديد أطيايف الامتصاصية، النفاذية، الإنعكاسية كدالة للطول الموجي وذلك لدراسة الثوابت البصرية المتمثلة في معامل الإمتصاص، معامل الإنكسار، معامل الخمود ، ثابت العزل بجزئيه الحقيقي و الخيالي اضافة الي خصائص متمثلة في فجوة الطاقة الضوئية و الموصلية الضوئية و الكهربائية. أشارت الدراسة أن اقصي قيمة لمعامل الإمتصاص $4.63 \times 10^3 \text{ cm}^{-1}$ كانت للعينة 1.0 مول عند ذروة بطول موجي 270 nm بينما كانت $1.34 \times 10^3 \text{ cm}^{-1}$ للعينه 0.1 مول لنفس الطول الموجي. أوضحت الدراسة أن كل العينات لها معامل إنكسار يساوي 2.159 عدا العينتان 0.1مول و العينه

0.2 مول لهما معاملا إنكسار 2.044 و 2.128 علي التوالي وهذه النتيجة قريبة من القيمة النظرية 2.004. فيما يتعلق بفجوة الطاقة الضوئية نجد أن الدراسة أشارت الى أن العينة 0.1 مول لأكسيد الزنك النانوي لها فجوة طاقة ضوئية كبيرة تساوي 3.889 eV و العينه 1.0 مول لها فجوة طاقة تساوي 3.443 eV مما تشير الى موصلية ضوئية جيدة. هذه النتيجة أثبتت ان مع زيادة تركيز محلول اسيتيت الزنك يقل مقدار فجوة الطاقة الضوئية. إضافة الى ذلك نجد أن الدراسة وجدت أن الموصلية الضوئية تساوي $1.34 \times 10^{11} \text{ sce}^{-1}$ للعينات 1.0 ، 0.9 ، 0.8 ، 0.7 مول التي تشيرالي إستجابة ضوئية عالية ، أما العينات 0.1 ، 0.2 ، 0.3 ، 0.4 ، 0.5 ، 0.6 مول نشترك في ذرة بطول موجي 268 nm ولها موصلية ضوئية مختلفة $7.48 \times 10^{10} \text{ sec}^{-1}$ ، $9.01 \times 10^{10} \text{ sec}^{-1}$ ، $1.17 \times 10^{11} \text{ sec}^{-1}$ ، $1.125 \times 10^{11} \text{ sec}^{-1}$ ، $1.309 \times 10^{11} \text{ sec}^{-1}$ علي التوالي.

Contents

| Titles of contents | page |
|--|------|
| Chapter One -Introduction | 1 |
| 1.1 General Introduction | 1 |
| 1.2 Motivation, aim and objectives of this Thesis | 3 |
| 1.3 Thesis Outlines | 4 |
| Chapter Two - Literature Reviver and Previous Works | 5 |
| 2.1 Introduction | 5 |
| 2.2 Properties of ZnO | 6 |
| 2.2.1 Physical and chemical Properties of ZnO | 6 |
| 2.2.2 Crystal Structure of ZnO | 7 |
| 2.2.3 Mechanical Properties of ZnO | 8 |
| 2.2.4 Electrical Properties | 8 |
| 2.2.5 Optical Properties | 9 |
| 2.3 Application Fields of ZnO | 9 |
| 2.3.2 Medical uses | 10 |
| 2.3.3 Food Additives | 10 |
| 2.3.4 Anti Corrosive Coatings | 10 |
| 2.3.5 Electronic Applications | 11 |
| 2.3.6 Usage of the ZnO Based Solar Cells | 11 |
| 2.4 Synthesizing Methods | 12 |
| 2.4.1 Sol-Gel Method | 12 |
| 2.4.2 Chemical Vapor Deposition (CVD) | 13 |
| 2.4.3 Hydrothermal and Solvothermal Process | 13 |
| 2.4.4 Controlled Precipitation | 14 |
| 2.5 Previous Works on the synthesized ZnO nanostructures by using sol-gel method | 15 |
| Chapter Three - Material and Method | 19 |
| 3.1 The experiment | 19 |
| 3.2 Characterization Techniques and Instruments | 20 |
| 3.3 Structural Analysis | 21 |
| 3.3.1 X-ray Diffraction Analysis | 21 |
| 3.3.2 Fourier Transform Infrared Spectrophotometer (FTIR) | 22 |
| 3.3.3 Surface and Morphological Analysis | 24 |
| 3.3.3.1 Scanning electron microscope | 24 |
| 3.3.4 UV-Visible Spectroscopy | 26 |
| Chapter Four- Results and Discussion | 28 |
| 4.1 Introduction | 28 |
| 4.2 Crystal Structure and Morphology | 28 |
| 4.2.1 X-ray Diffraction Analysis | 28 |
| 4.2.2 The relation between the concentrations and : dislocation dencity, crystal | 41 |

| | |
|---|----|
| size, d- spacing and average lattice constant | |
| 4.3 Scanning Electron Microscopy (SEM) Analysis of ZnO samples | 44 |
| 4.4 Fourier Transform Infrared Spectrophotometer (FTIR)analysis | 49 |
| 4.5The Optical properties of ZnO nanostructures | 53 |
| 4.5.1 The Absorbance | 53 |
| 4.5.2 The Transmittance | 54 |
| 4.5.3 The Reflectance | 55 |
| 4.5.4 Absorption Coefficient | 56 |
| 4.5.5 Extinction Coefficient (K). | 57 |
| 4.5.6 The Refractive Index (n) | 58 |
| 4.5.7 The Optical Energy Gap (Eg) | 59 |
| 4.5.8 Real Dielectric Constant (ϵ_1) | 61 |
| 4.5.9 Imaginary Dielectric Constant (ϵ_2) | 62 |
| 4.5.10 The Optical and The Electrical Conductivity | 63 |
| Chapter Five | 65 |
| Conclusion and Recommendations | 65 |
| References | 68 |
| Appendix: publishing papers arising out of this thesis | 71 |

List of Tables

| Titles of Tables | page |
|---|------|
| Table 2.1: Physical Properties of ZnO | 6 |
| Table 3.1: shows the amounts of zinc acetate in molar used to synthesized ZnO nanostructures | 19 |
| Table 4.1: shows the parameters of 2-Theta, Miller indices and d – spacing of the ten samples of ZnO respectively | 40 |
| Table 4.2: shows some crystallite lattice parameters of all samples of as-synthesized ZnO nanostructures | 41 |
| Table 4.3: FTIR Parameters in (cm^{-1}) of the ten samples of synthesized ZnO nanostructures using different concentration of zinc acetate | 53 |

List of Figures

| | Figures | page |
|--|---------|------|
| Figure (1.1): shows (a) 3D-structure; (b) 2D-structure; (c) 1D-structure and (d) 0D-structure [4], https://nccr.iitm.ac.in/2011.pdf | | 2 |
| Figure (2. 1): ZnO structures: (a) hexagonal wurtzite, (b) cubic zinc blende and (c) cubic rocktsalt | | 7 |
| Figure (2.2): $(\alpha h\nu)^2$ versus photon energy plot of (A) pure ZnO thin films (B) with different doping concentration of Fe, Selam et al [78] | | 15 |
| Figure (2.3): X-ray diffraction patterns of ZnO thin film prepared <i>after different</i> aging time, Sara et al [13] | | 16 |
| Figure (2.4): XRD pattern of ZnO Nr with hydrothermal process and the bandgap that grew from the 2-methoxyethanol seeded layer, Foo et al [79] | | 17 |
| Figure (2.5): Experimental characteristics (current -voltage) of pure ZnO at various temperatures, Khalaf et al [14] | | 17 |
| Figure (2.6): shows the variation of refractive index with wavelength and the bandgap of ZnOfabricated by Hussien et al [80] | | 18 |
| Figure (3.1): shows a milky solution of zinc Acetate for preparing sample3 | | 19 |
| Figure (3.2) : Shows the as-obtained transparent solutions of the ten samples | | 20 |
| Figure (3.3): Reflection of x-rays from two planes of atoms in a solid | | 21 |
| Figure (3.4): shows the Fourier transform Infrared Spectroscopy https://en.wikipedia.org/wiki/Fouriertransform_infrared_spectroscopy | | 23 |
| Figure (3.5): (a) and (b) show schematics diagram for Scanning Electron Microscope (SEM). https://www.purdue.edu/ehps/rem/rs/sem.htm . | | 25 |
| Figure (3.6): shows the Ultraviolet/Visible (Uv vis) spectroscopy. https://www.researchgate.net/figure/17-Spectrophotometre-UV-Vis-VARIAN-Cary-100-Scan_fig16_278826646 | | 27 |
| Figure (4.1): The XRD patterns of the as- synthesised ZnO nanostructures fo sample 1.0 M | | 29 |
| Figure (4.2): The XRD patterns of the as- synthesised ZnO sample 0.9 M nanostructures | | 30 |
| Figure (4.3): The XRD patterns of the as- synthesised ZnO sample 0.8 M nanostructures | | 31 |
| Figure (4.4): The XRD patterns of the as- synthesised ZnO sample 0.7 M nanostructures | | 32 |
| Figure(4.5): The XRD patterns of the as- synthesised sample ZnO 0.6 M nanostructures | | 33 |
| Figure (4.6): The XRD patterns of the as- synthesised ZnO sample 0.5 M nanostructures | | 34 |
| Figure (4.7): The XRD patterns of the as- synthesised ZnO sample 0.4 M nanostructures | | 35 |
| Figure (4.9): shows the X-ray diffraction patterns of the synthesized ZnO 0.2 M nanocrystals | | 36 |
| Figure (4.9): The XRD patterns of the as- synthesised ZnO sample 0.2 M nanostructures | | 37 |
| Figure(4.10): The XRD patterns of the as- synthesised ZnO 0.1 M sample nanostructures | | 38 |
| Figure (4.11): represents the XRD charts of the ten samplesof as-synthesized ZnO nanostructures using different concentrations of zinc acetate | | 39 |
| Figure (4.12): The relation between the Density and the concentrations of Ten samples of the synthesized ZnO nanostructures | | 41 |

| | |
|---|----|
| Figure (4.13) The relation between Crystlite size and the concentrations of zinc acetate for the ten samples that of synthesized ZnO nanostructures | 42 |
| Figure (4.14): The relation between d- Spacing and concentrations of zinc acetate for the ten samples of as-synthesized ZnO nanostructures | 43 |
| Figure (4.15) The relation between Average Lattice Constant and concentration of zinc acetate for the ten samples of as- synthesized ZnO nanostructures | 43 |
| Figure (4.16): shows the SEM images for samples 1.0 M and 0.9 M respectively | 45 |
| Figure (4.17): shows the SEM images for samples 0.8 M and 0.7 M respectively | 46 |
| Figure (4.18): shows the SEM images for samples 0.6 M and 0.5 M respectively | 47 |
| Figure (4.19): shows the SEM images for samples 0.4 M and 0.3 M respectively | 48 |
| Figure (4.20): shows the SEM images for samples 0.2 M and 0.1 M respectively | 49 |
| Figure (4.21) : represents the FTIR spectrums of as-synthesized ZnO nanostructures for the ten samples symbolized in molar form 1.0 M to 0.1 M respectively | 52 |
| Figure (4.22) : FTIR spectrum of the ten samples of as-synthesis ZnO film nanostructures | 52 |
| Figure (4.23): shows the relation between absorbance and wavelengths of the ten samples of as- synthesised ZnO thin film nanostructures | 54 |
| Figure(4.24): Indicates the relation between transimission and wavelengths of the ten samples of as-synthesised ZnO thin film nanostructures | 55 |
| Figure (4.25): shows the relation between reflection and wavelengths of Ten samples of as-synthesized ZnO film nanostructures | 56 |
| Figure (4.26): shows the relation between the absorption coefficient and the wavelengths of ten samples of as-synthesiezes ZnO films nanostructures | 57 |
| Figure (4.27): shows the relation between the extintion coefficient and wavelengths of ten samples of as-synthesiezes ZnO films nanostructures | 58 |
| Figure (4.28): represents the refractive index of the ten samples of as-synthesised ZnO nanostructures as function of wavelength | 59 |
| Figure (4.29): Plot of $(\alpha h\nu)^2$ versus the photon energy ($h\nu$) for ZnO nanostructures synthesized by using different concentrations of zinc acetate | 60 |
| Figure (4.30): shows the relation between the real dielectric constant and the wavelengths of the ten samples of as-synthezised ZnO films nanostructures | 61 |
| Figure (4.31): The relation between imaganry dielectric constant and wavelengths of the ten samples of as-synthesized ZnO film nanostructures | 62 |
| Figure (4.32): Shows the relation between, (a) the optical conductivity and (b) electrical conductivity versus the wavelengths of ten samples of as-synthezied ZnO nanostructures | 64 |

Chapter One

Introduction

1.1 Background to Nanotechnology

Nanotechnology is an interdisciplinary field of the sciences of physics, chemistry and materials sciences, meant for the design and fabrication of nanomaterials and their applications. This branch of science is destined to understand the fundamental physical and chemical properties and the phenomenon of nanomaterials and nanostructures, and because of the novel applications of nanomaterials, the science of nanomaterials has evolved as a frontline research area [1, 2]. Feynman pointed out the importance of nanotechnology at the annual meeting of the American Physical Society in 1959, in the classic science lecture entitled “There is plenty of room at bottom”. In the last three decades, many discoveries and inventions have been made in the field of nanoscience in terms of fabricating new materials and utilizing them for applications. Various new experimental techniques, with unique and desired properties of nanomaterials fabrication have been discovered.

Considerable research efforts with different synthesis methods have given birth to different class of nanomaterials, typically classified into four categories based on their dimensionality: Zero dimensional (0D), one dimensional (1D), two dimensional (2D) and three dimensional (3D) Figure (1.1). Quantum dots and the individual molecules fall in the 0-dimensional structures where the nanoparticles are isolated from each other and the electrons are confined in 3D [3-5]. One dimensional nanostructures (nanowires, nanorods, nanotubes, nanobelts ..etc), where at least one of the dimension goes in the range of nanoscale order are being highly utilized and have versatile application in the nanodevice fabrications. Thin nano films lie in the two dimensional structures and are studied extensively for the utilization of nanodevice application [6-8]. Three-dimensional nanomaterials include powders, fibrous, multilayer and polycrystalline materials in which the 0D, 1D and 2D structural elements are in close contact with each other and form interfaces. An important type of three-dimensional nanostructured materials is a compact

or consolidated (bulk) polycrystal with nanosize grains, whose entire volume is filled with those nanograins.

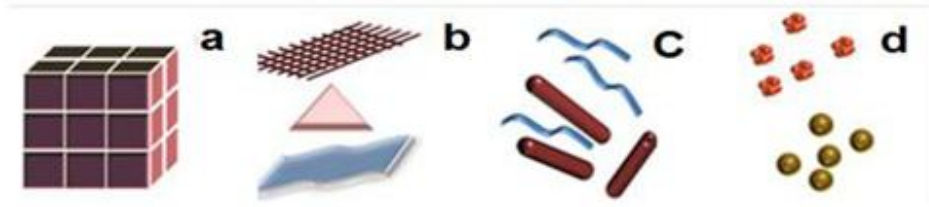


Figure 1.1: shows (a) 3D-structure; (b) 2D-structure; (c) 1D-structure and (d) 0D- structure [4],<https://nccr.iitm.ac.in/2011.pdf>

Among those, semiconductors are one of the richest classes of nanomaterials. A semiconductor is a material with electrical conductivity due to electron flow intermediate in magnitude between that of an insulator and a conductor. Semiconductor has governed a significant role in progressing research in nanoscience and nanotechnology, which results in novel classes of semiconductor materials. Usually in conductors current is considered to flow due to electrons only but here in semiconductor materials it is caused by both electron as well as hole movements. Semiconductor materials do not belong only to crystal solids but are of the nature of amorphous and liquids too. The electronic properties and the conductivity of semiconductor can be changed in a controlled manner by adding very small quantities of other materials called dopants.

The field of nano is expected to open new avenues for science and technology. Preparation and applications of the metal oxide nanostructures is one of the classes belonging to semiconducting nanomaterials and nanotechnology. Metal oxide proved to be very promising for a variety of practical applications. The good thermal and chemical stability of these inorganic materials enable them to be widely used. Metal oxides play a very important role in many areas of chemistry, physics, and materials science [9-12]. These metal oxides have unique positions due to their piezoelectric, transparent conducting properties, optical transmittance and high electrical conductivity. These

properties make metal oxide an ideal for applications in thin film hetero junction solar cells in window layers, and transparent conducting electrodes in flat panel displays.

Zinc oxide (ZnO), belong to the family of metal oxides and has a unique position among semiconducting oxides due to its own properties and wide range of applications. These properties make it an ideal candidate for many applications like transparent conducting electrodes in flat panel displays and window layers in solar cells [1-4]. ZnO has a wide band gap 3.37 eV to 4 eV [3,4] and a large exciton binding energy (60 meV) and exhibits many potential applications in areas such as laser diodes, solar cells, gas sensors, optoelectronic devices. Also this wide band gap enabling high temperature and power operations, reducing electronic noise, making sustenance in large electric fields possible and raising breakdown voltages [5-7]. Therefore, these excellent properties of Zinc Oxide (ZnO) attract the attention towards the synthesis of ZnO nanostructures which can play an important role to enhance and to improve the optical and electrical applications when comparing to ZnO bulk structures.

1.2 Objectives of the Thesis

There are many methods has been used to synthesize ZnO nanostructures, some of them are described in section (2.4). These methods have been successfully used for producing nanostructures of ZnO in form of nanowires, nanorods, nanoparticles etc [13, 14, 15].

The aim of this study: Simple method like sol-gel process that leads to possible low cost and pure products and easy film processing on a variety of substrates are of great attracted attention for researchers and commercial applications to synthesize ZnO nanostructures. Consequently, the present thesis focusing on: synthesis of ZnO nanostructures with purity and high productivity via sol- gel method using different concentrations of zinc acetate, searching for optimal conditions for commercial applications.

Investigation of the structure and the morphology and optical properties, based on X-ray Diffraction (XRD) analysis, Scanning Electron Microscopy (SEM) imaging, and Fourier Transform Infrared Spectrophotometer (FTIR) and UV spectroscopy on the composites of ZnO nanostructures are very important to achieve the main objectives in this thesis. These main objectives are:

- To Synthesize ZnO films nanostructures by using different concentrations of zinc acetate.
- To characterize ZnO in the presence of different concentrations of zinc acetate.
- To examine whether the variations of the concentrations of zinc acetate has any effect on the as-synthesized ZnO nanostructures in terms of structure, morphology and optical properties.

1.3 Thesis Outlines

A brief outline of the whole thesis is presented in the following: The thesis starts with a short chapter (Chapter One) introducing a fundamental concepts of the nanotechnology with a brief background on metal oxides. Chapter two gives short descriptions concerning the literature view of ZnO material including its properties, some synthesizing methods and some previous works used to synthesized ZnO nanostructures via sol-gel process. Chapter three comprise the general experimental methodology used in our research works as well as provides simple descriptions about the techniques applied to synthesize and characterize the samples reported in the present work. Chapter four is the important and the core part of the thesis, deals with the discussion on the crystallite and the properties of as-synthesized ZnO thin films nanostructures. Finally, the general conclusion about all the presented work is reported in chapter five.

Chapter Two

Literature Review and Previous Works

2.1 Introduction

Zinc oxide with the chemical formula of ZnO is one of the well-known semiconductor material. For only 2018, with the key word ZnO, the data collections in Web of Science give more than 6000 scientific studies within the various research areas including physics, chemistry, nanotechnology and material science. However, this does not mean that ZnO is newly discovered material. The history of ZnO goes back to ancient age. The ancients discovered the production of the first brass-metal and the medical equipment's made with purified ZnO. In the last few decades, the interest in this fascinating chemical compounds reemerges with the usage ZnO powder as an industrial processing chemical and a white paint pigment. In addition, for over one hundred years, polycrystalline form of ZnO has been used in a variety of applications such as electronic materials, gas sensors, cosmetic and pigment industry [16, 17]. The focused interest in this material started in the 1920s with the first utilization of ZnO for its semiconductor properties. With the discovery of attractive semiconductor properties of ZnO during 1950s, researchers focused on the bulk ZnO growth and applications [18]. During 1960s, synthesis of ZnO thin film has been extensively studied due to potential applications of ZnO thin film in the sensor and catalyst applications [19]. Since 1990s, a major research interest has been on the synthesis of ZnO nanostructures by different growth methods [20, 21]. Nowadays, the world wide afford in the fabrication of the high quality single crystal ZnO for the ZnO-based electronic and optoelectronic devices encouraged the researchers and provided to document hundreds of papers about ZnO structure.

ZnO is a wide bandgap semiconductor with direct bandgap energy of 3.4 eV which provides to operate in the blue and ultra-violet optical devices [20, 22]. In addition, it has large exciton binding energy of 60 meV which gives ZnO several advantages over gallium nitride (GaN, 25 meV) such as better radiation resistance for devices used in space and nuclear applications and simpler and cost effective crystal growth methods [23]. Large exciton binding energy of ZnO provides to increase the exciton stability and

enhance luminescence efficiency by increasing the possibility of radiative recombination. Therefore, ZnO is a very interesting semiconductor and has been extensively used in electronic and optoelectronic devices [24].

2.2 Properties of ZnO

2.2.1 Physical and chemical Properties of ZnO

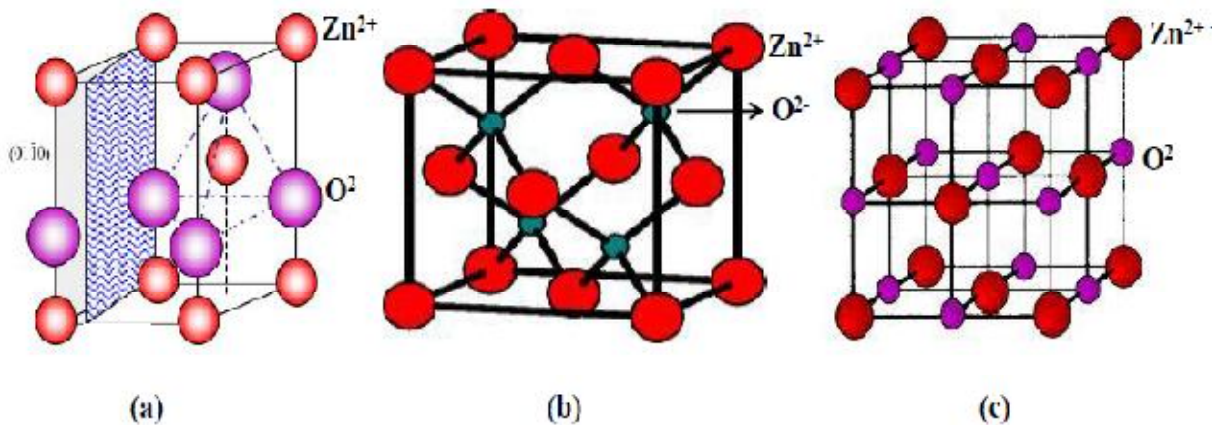
ZnO is an inorganic compound which usually appears as a odorless white powder in the bulk form. In nature, mineral form of ZnO is zincite which contains impurity phases such as iron and manganese and appears as yellow or red according to impurity content [25]. The basic physical and chemical properties of ZnO are listed in Table 2.1.

Table 2.1: Physical Properties of ZnO [26,44,45].

| Property | Value |
|---------------------------------|---|
| Molecular formula | ZnO |
| Molar mass | 81.4084 g/mol |
| Appearance | Amorphous white or yellowish white powder. |
| Odour | Odourless |
| Density | 5.606 g/cm ³ |
| Melting point | 1975 °C |
| Boiling point | 2360 °C |
| Solubility in water | 0.16 mg/100 mL |
| Refractive index | 2.0041 |
| Lattice Constants | $a_o = 3.2469 \text{ \AA}$, $c_o = 5.2069 \text{ \AA}$ |
| Relative Dielectric Constant | 8.66 |
| Energy Gap | 3.4 eV Direct |
| Intrinsic Carrier Concentration | $< 10^6 /\text{cc}$ |
| Exciton Binding Energy | 60 meV |
| Electron effective mass | 0.24 |
| Electron mobility (at 300 K) | 200 cm ² /V.sec. |
| Hole Effective mass | 0.59 |
| Hole mobility (at 300 K) | 5-50 cm ² /V.sec |

2.2.2 Crystal Structure of ZnO

There are three forms of ZnO crystals structures, hexagonal wurtzite, cubic zinc blende, and cubic rocksalt structures Figure (2.1). The wurtzite structure is most stable at ambient conditions and thus most common. The zincblende form can be stabilized by growing ZnO on substrates with cubic lattice structure of $a = 0.46$ nm and also can be form in local cubic structure with unit cell of $a = 0.8$ nm. In both cases, the zinc and oxide centers are tetrahedral. The rocksalt (NaCl-type) structure is only observed at relatively high pressures about 10 GPa. Hexagonal and zinc blende polymorphs have no inversion symmetry (reflection of a crystal relatively any given point does not transform it into itself). This and other lattice symmetry properties result in piezoelectricity of the hexagonal and cubic zinc blende ZnO, and in pyroelectricity of hexagonal ZnO [26-33]. A more stable state of ZnO is wurtzite structure having hexagonal unit cell with the lattice parameters $a = 0.3296$, and $c = 0.52065$ nm. The oxygen anions and Zn cations form a tetrahedral unit. The entire structure lacks central symmetry. The structure of ZnO can be simply described as a number of alternating planes composed of tetrahedrally coordinated O^{2-} and Zn^{2+} ions, stacked alternatively along the c-axis [34-38] as shown in the Figure (2.1a).



Figure(2. 1): ZnO structures: (a) hexagonal wurtzite, (b) cubic zinc blende and (c) cubic rocksalt [39,40].

2.2.3 Mechanical Properties of ZnO

It is relatively a soft material having a hardness of 4.5 on the Mohs scale approximately. Its high heat capacity and heat conductivity with low thermal expansion and high melting temperatures makes it beneficial for ceramics. It has one of the highest piezoelectric tensor compared to other III-V semiconductors such as GaN and An. This property makes it important for many piezoelectrical applications, which require a large electromechanical coupling.

2.2.4 Electrical Properties

As a direct and wide band gap semiconductor with a large exciton binding energy (60meV), ZnO is representing a lot of attraction for optoelectronic and electronic devices. For example, a device made by material with a larger band gap may have a high breakdown voltage, lower noise generation, and can operate at higher temperatures with high power operation. The performance of electron transport in semiconductor is different at low and high electric field. At sufficient by low electric fields, the energy distribution of electrons in ZnO is unaffected much, because the electrons can't get much energy from the applied electrical field, as compared with their thermal energy. So the electron mobility will be constant because the scattering rate, which determines the electron mobility, doesn't change much. When the electrical field is increased, the energy of the electrons from the applied electrical field is equivalent to the thermal energy of the electron. The electron distribution function changes significantly from its equilibrium value. These electrons become hot electrons, whose temperature is higher than the lattice temperature. So there is no energy loss to the lattice during a short and critical time. When the electron drift velocity is higher than its steady state value, it is possible to make a higher frequency device. Usually most of the ZnO materials are of n- type character, p-type doping of ZnO is relatively difficult. But this limitation of p-type doping does not restrict the applications of ZnO in electronic and optoelectronic [41].

2.2.5 Optical Properties

ZnO material has wide applications in the optical field such as, nanorods can be used in lasers for fast optical pumping and hence produce high power laser beams. In the near ultra violet and in visible regions, due to its wide band gap character ZnO material displays unique properties. Excitonic emissions have been observed from the PL spectra of ZnO materials. It has been also observed that on the confinement of quantum size of ZnO nanomaterials, the exciton binding energy increases but it has also been observed at the same time that the intensity of green emission increases very much due the decrease in the diameter of the ZnO nanorod diameters. This is due to large ratio of surface to volume factor of nanowires favouring higher level of defects and surface combinations. Quantum confinement was also reported to be responsible for blue shift in the near UV emission peak in the ZnO nanobelts. Other application include and are not limited to optical fibres, solar cells , surface acoustic devices etc. [41-43]. The physical properties of the ZnO material are given as in the table 2.1 [26,44,45].

2.3 Application Fields of ZnO

ZnO has got a wide range of applications ranging from cosmetics to optoelectronic devices.. The reactivity of ZnO makes it ideal to be used as a precursor for obtaining other compounds of Zn. Zinc Oxide has proved to be a benefit for materials science as it has got a combination of unique properties like UV absorption, anti microbial properties, steady thermal and optical properties.

General application fields can be classified as; electronics and electrotechnology industries (gas sensors, solar cells, field effect transistors, light emitting diodes, varistors and spintronic devices), photocatalyst industry, textile industry, rubber industry and pharmaceutical and cosmetic industries [46-52]. This study mentioned some application fields of ZnO nanocomposites.

2.3.1 Rubber Manufacture

The rubber industry is responsible for consuming about 50% of the ZnO that is produced globally. ZnO along with stearic acid are a must for activating the process of vulcanization in rubber manufacture. Rubber curing becomes faster and more controlled when a combination of these two substances is used. It is also a very important additive in car tyres. It helps in improving their thermal conductivity which helps the tyres to dissipate heat quickly when they are in motion thereby increasing their life span [52].

2.3.2 Medical Uses

A mixture of ZnO with 0.5% Fe₂O₃ is known as calamine and is used in manufacturing Calamine lotions. Fine particles of ZnO have anti microbial and deodorizing qualities and hence they are used for packaging purposes. These properties along with its ability of neutralizing acids makes it ideal for use in antiseptic creams, healing creams etc. they are also an important component of toothpastes and dental prosthetics. Due to its ability to absorb ultraviolet light, ZnO is also used in sunscreens and sun-blocks to prevent sunburns. ZnO is also used in the making of cigarette filters as it helps in removing harmful substances like H₂S and HCN without affecting the flavor [52, 63].

2.3.3 Food Additives

ZnO is usually added to food products as a source of Zn which is considered to be a necessary nutrient as it helps in the performance of various physiological activities like growth and proper functioning of the sexual organs. ZnO is also added to fodder as a Zn supplement for livestock. Zinc oxide is used to manufacture zinc gluconate which is nowadays found in cold prevention lozenges.

2.3.4 Anti Corrosive Coatings

Zinc oxide is an excellent inhibitor of fungi, mildew and mould [65]. Paints which have ZnO are usually used as anti corrosive coatings for various metals like galvanized Zn which is especially hard to protect as it makes organic coatings brittle and unsuitable for adhesion [64]. ZnO paints on the other hand maintain their flexibility and adhesive properties for years on end. The UV blocking abilities of ZnO also play an important role in improving the resilience of the paint. Unlike some lead pigments that are available

commercially, ZnO is impervious to the effect of sulfur compounds that are present in the atmosphere [46, 50].

2.3.5 Electronic Applications

The wide band gap of ZnO enables it to be used for the purpose of making the light emission diodes (LEDs) and laser diodes. Transparent thin-film transistors (TTFT) can also be produced with ZnO. Nanorod sensors made of ZnO are devices that detect fluctuations in electric current passing through the wires as a result of the adsorption of gas molecules. The nanorods can be made partial towards H₂ gas by sputtering Pd clusters on the surface which help in dissociating the H₂ molecules thereby increasing the sensitivity of the nanorods. H₂ concentrations up to 10 ppm can be detected at room temperature without any response to O₂ [40, 52].

Properties like biocompatibility have enabled ZnO to be used as a biomimic material to modify and immobilize biomolecules. As Field-effect transistors (FETs), they can function without even a p-n junction thus bypassing doping problems. This is why some FETs use nanorods made of ZnO as conducting channels. ZnO is also used in making Zn-C dry cells, Ni-Cd oxide batteries, Zn-Ag oxide batteries and also some secondary batteries. Another major area of ZnO application is fuel cell where it is used to make various parts like the electrodes and sometimes also as the fuel. It can also act as a photo catalyst in places like the solar cell [52, 53].

2.3.6 Usage of the ZnO Based Solar Cells

Solar cell is an electronic device which directly converts sunlight into electricity. The working principle of solar cell device is based on the photovoltaic effect. A well-known photovoltaic device is the single-crystalline silicon solar cells which operate on the principle of the p-n junctions. However due to high material cost of the single-crystalline silicon solar cell, thin film solar cells have been studied worldwide. With the development of the dye synthesized solar cells (DSSCs), the usage of the ZnO based DSSCs has extensively increased since although lower conversion efficient (0.4-5.8 %) than that of 11% for TiO₂, easily crystallization and anisotropic growth makes ZnO a distinguished alternative to TiO₂ [54-56]. Morphology of ZnO nanostructures used in

DSSC is also important for the overall device efficiency. Ko et al.[56], reported that special nanoforest morphological ZnO nanostructures with high density, long branched treelike nanowires show a significantly improved DSSC power conversion efficiency and five times higher light conversion efficiency than that of ZnO nanowires

2.4 Synthesizing Methods

Keeping in view, and over the years, ZnO nanostructures can be synthesized by several methods such as sputtering technique, Vapour Deposition, Pulsed laser Deposition (PLD), metal organic Chemical Vapour Deposition (MOCVD), Hydrothermal Growth process, oxidation and Vapour liquid-Solid process...etc. Some of these methods are extensively used because are simple and low cost product of ZnO nanostructure [59-61]. Below presented brief description about some methods used to synthesize ZnO nanostructures.

2.4.1 Sol-Gel Method

Sol-gel method known as chemical solution deposition is based on the hydrolysis of liquid precursors and formation of colloidal sols. The technique is simple, low cost and common method used to fabricate one-dimensional metal oxides nanostructures. The formation of nanosized semiconductor or metal elements permits system with peculiar optical and electrical properties. The Sol-gel methods a well-established colloidal chemistry technology, which offers possibility to produce various materials with novel, predefined properties.

In this process a chemical transformation of a liquid (the sol) into a gel state take place with subsequent post-treatment and transition into solid oxide material. The main benefits of sol-gel processing are the high purity and uniform nanostructure achievable at low temperatures [60-62]. One of the applications of this process is: synthesizing ceramic materials and metal oxides of high purity and homogeneity in comparison with other traditional processes of fusion of oxides.

On the other hand, the study may use a wet chemical synthesis technique as bottom up method. This procedure is simple and low cost as well. In this method different concentrations of soluble starch or other soluble material can be used to make a solution

with distilled water. Then an appreciated amount of chemical compound contains the Zinc element and other chemical compound contains the doping element. These composed materials will add to the starch solution under a magnetic stirring for esteemed time. The next step, the surfactant will be added drop by drop under a magnetic stirring. Then this solution will centrifuge before discard out. The as-obtained products should wash several times to remove the remaining byproducts. Finally, the as-product will dry at low temperature.

2.4.2 Chemical Vapor Deposition (CVD)

This technique (CVD) is widely used for preparing epitaxial structures by depositing atoms on a wafer substrate. For various thin film growths, this method has been extensively used. The operational principle is very simple. For the specific crystal growth, the desired atoms, which are combine with a particular complex organic gas molecules are passed over a hot semiconductor wafer. Due to heat, the complex organic molecules breakup and deposit the desired atoms layer by layer onto the substrate surface. The undesired remnants are removed or deposited on the walls of the reactor. By varying the composition of the gas, the crystal properties at almost atomic scale can be changed. Using this technique, layers of the precisely controlled thickness can be obtained, which is important for the fabrication of materials with specific optical and electrical properties [63-67].

2.4.3 Hydrothermal and Solvothermal Process

Solvothermal synthesis is a method for preparing a variety of materials such as metals, semiconductors, ceramics, and polymers. The process involves the use of a solvent under moderate to high pressure (typically between 1 atm and 10,000 atm) and temperature (typically between 100 °C and 1000 °C) that facilitates the interaction of precursors during synthesis. If water is used as the solvent, the method is called 'hydrothermal syntheses. The synthesis under hydrothermal conditions is usually performed below the supercritical temperature of water (374 °C). The process can be used to prepare structures with various morphologies including thin films, bulk powders, single crystals, and nanocrystals. In addition, the morphology (sphere (3D), rod (2D), or

wire (1D)) of the crystals formed is controlled by manipulating the solvent supersaturation, chemical of interest concentration, and kinetic control. The method can be used to prepare thermodynamically stable and metastable states including novel materials that cannot be easily formed from other synthetic routes. Over the last decade, a majority (~80%) of the literature concerning solvothermal synthesis has focused on nanocrystals; therefore, this review will highlight some advances in nanocrystalline, solvothermal synthesis [68]. An example of a hydrothermal reaction is the synthesis of zinc oxide as proposed by Chen et al [69], using the reagents ZnCl_2 and NaOH in a ratio of 1:2, in an aqueous environment. A hydrothermal process was also used by Ismail et al [70], using $\text{Zn}(\text{CH}_3\text{COO})_2$ and NaOH was carried out in the presence of hexamethylenetetramine (HMTA), at room temperature. The shape of the particles is also affected by the time and temperature of the hydrothermal process. With an increase in time, temperature and surfactant concentration, the size of the particles increases. Musić et al [71] determined the effect of chemical synthesis on the size and properties of ZnO particles. A suspension obtained from a solution of $\text{Zn}(\text{CH}_3\text{COO})_2 \cdot 2\text{H}_2\text{O}$ and neutralized using different quantities of a solution of NH_4OH underwent hydrothermal treatment in an autoclave at a temperature of $160\text{ }^\circ\text{C}$. A number of studies [72-74] have shown that the use of microwave reactors in hydrothermal synthesis processes brings significant benefits.

2.4.4 Controlled Precipitation

Controlled precipitation is a widely used method of obtaining zinc oxide due to the precession of the properties of the obtained product. The method involves fast and spontaneous reduction of a solution of zinc salt using a reducing agent, to limit the growth of particles with specified dimensions, followed by precipitation of a precursor of ZnO from the solution. Zinc oxide with monodispersed particle size distribution and high surface area are obtained by controlled precipitation from aqueous solutions of zinc chloride and zinc acetate [72] Hong et al. reported that nano ZnO can be prepared by using zinc acetate [$\text{Zn}(\text{CH}_3\text{COO})_2 \cdot \text{H}_2\text{O}$], ammonium carbonate $(\text{NH}_4)_2\text{CO}_3$ and poly ethylene glycol [76] . Jia et al [77] reported that, in situ crystallization transformation

from Zn(OH)₂ to ZnO is demonstrated. Transformation from ε-Zn(OH)₂ to ZnO followed two mechanisms: dissolution– re-precipitation and in situ crystallization transformation involving dehydration and internal atomic rearrangements. From a fundamental point of view, these findings provide new insights into the growth of ZnO crystals.

2.5 Previous Works on the synthesized ZnO nanostructures by using sol-gel method.

This section introduces some papers talk about synthesizing of ZnO nanostructures by using sol gel method. Interestingly, so far, there are many reports about synthesis of zinc oxide nanostructures (nanowires, nanorods and nanoparticles) by using sol gel method. In recent works, for example, Selam et al,2019[78] have successfully fabricated Pure and Fe-doped zinc oxide nanocrystalline films via a sol–gel method using spin coating process. The XRD results showed that ZnO has hexagonal wurtzite structure and the Fe ions were well incorporated into the ZnO structure. The optical band gap energy of spin-coated films in this paper decreasing as Fe doping concentration increased with maximum value of $E_g = 3.75$ eV Figure (2.2) . Also this study proved that the photocatalytic activity of samples ZnO increased with increasing the concentration of Fe.

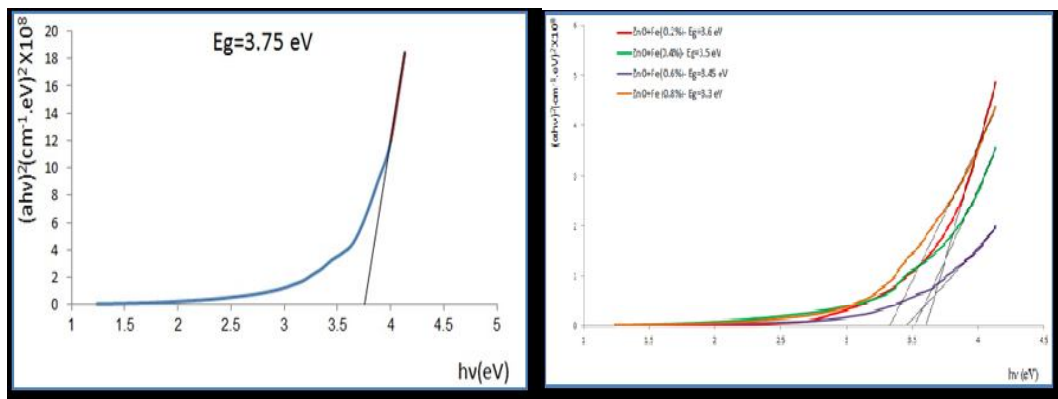


Figure (2.2): $(\alpha hv)^2$ versus photon energy plot of (A) pure ZnO thin films (B) with different doping concentration of Fe, Selam et al [78].

Also, Zinc oxide (ZnO) thin films were deposited on glass substrate by dip coating technique, Sara et al, 2015 [13]. The study found that the morphology of the films strongly depends on preparation route and deposition technique also the increase in sol

aging time resulted in a gradual improvement in crystallinity (in terms of peak sharpness and peak intensity) of the hexagonal phase for all diffraction peaks Figure (2.3). Interestingly, the sol aging time was found to be optimal to achieve smooth surface morphology, good crystallinity and high optical transmittance which were attributed to an ideal stability of solution.

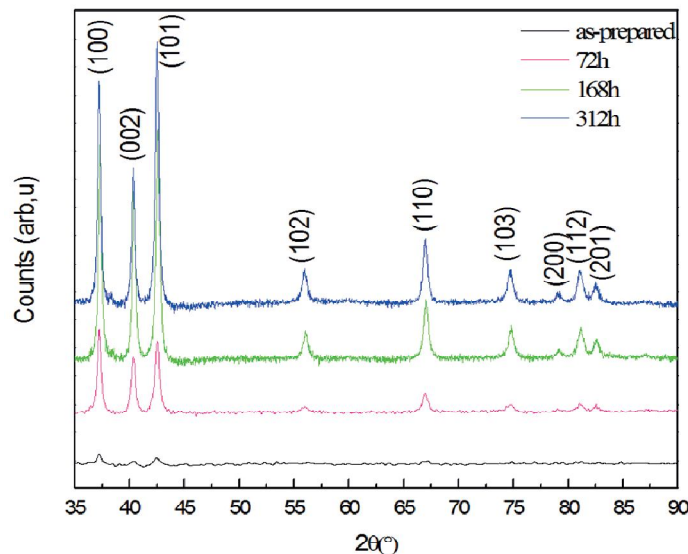
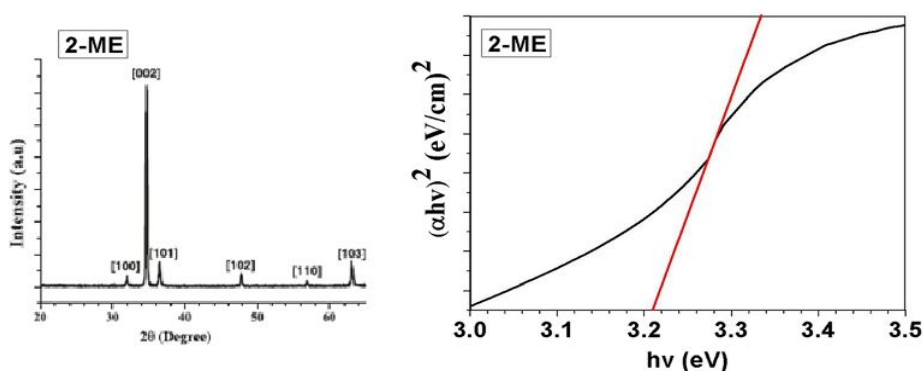


Figure (2.3): X-ray diffraction patterns of ZnO thin film prepared after different aging time, Sara et al [13].

Nanostructured zinc oxide (ZnO) nanorods (NRs) with hexagonal wurtzite structures were synthesized using an easy and low-cost bottom-up hydrothermal growth technique Foo et al, 2014 [79]. ZnO thin films have been prepared by using four different solvents, namely, methanol, ethanol, isopropanol, and 2-methoxyethanol, and then used as seed layer templates for the subsequent growth of the ZnO NRs. The results from XRD patterns showed that the synthesized ZnO NRs were single crystals and exhibited a preferred orientation along the (002) plane. Foo et al, shows the ZnO NRs that grew from the 2-methoxyethanol seeded layer exhibited the smallest grain size (39.18 nm), largest diffracted intensities on the (002) plane, and highest bandgap (3.21 eV) Figure(2.4).



Figure(2.4): XRD pattern of ZnO Nr with hydrothermal process and the bandgap that grew from the 2-methoxyethanol seeded layer, Foo et al [79].

Khalaf et.al, 2017 [14] and Jurablu et al 2015 [15]synthesized ZnO nanopwoder by sol-gel method using zinc acetate. They calcined the gel precursor at different temperature. From the XRD study, they found the ZnO oxide nanoparticles exhibited hexagonal wurtzite structure. The topographical information showed homogenous distribution of the nanoparticleswith average size of 22 nm that agree with XRD data 2-30 nm. Also the study addressed that the powder zinc oxide in nano scale without impurities offers moderately good quality factors of the varistor like high breakdown voltage ($V=450V$) and non-linear coefficient ($\alpha=30$) Figure (2.5).

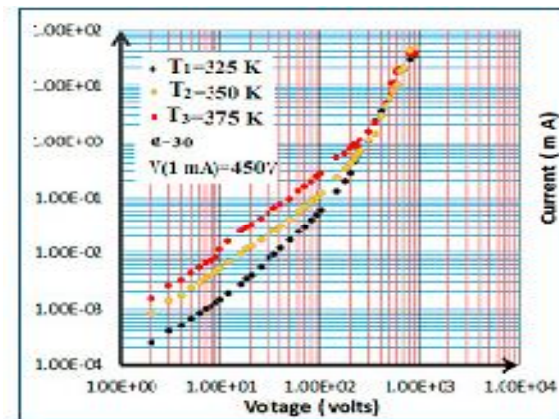
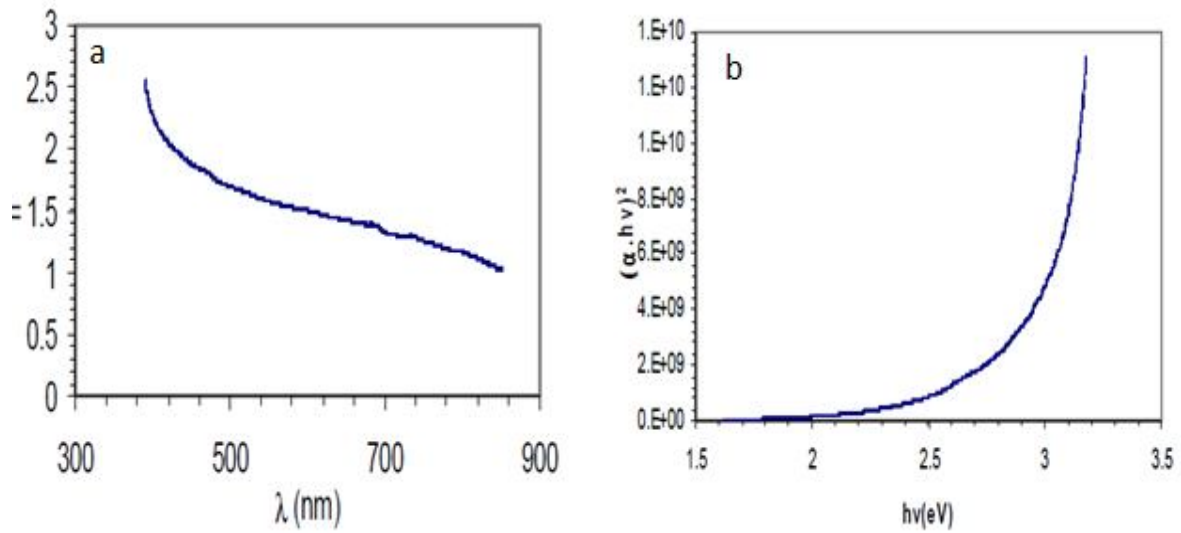


Figure (2.5): Experimental characteristics (current -voltage) of pure ZnO at various temperatures, Khalaf et al [14].

Hussein et al, 2011 [80]fabricated the ZnO thin film by using Sol-gel technique. Zinc acetate, isopropanol, and monoethanolamine were used as the precursors. Hussien and his group calculated the absorption, transmittance, absorption coefficient α , and the films thickness (d) from the obtaining interference of transmittance spectra. They found

that the energy band gap of the films was evaluated as 3.04 eV and the refractive index decreased with increasing the wavelength Figure (2.6).



Figure(2.6): shows the variation of refractive index with wavelength and the bandgap of ZnO fabricated by Hussien et al [80].

Chapter Three

Materials and Method

3.1 The Experiment

The precursors that utilized to synthesize ZnO nanostructures are achieved by using different concentrations of Zinc acetate dehydrate $Zn(CH_3COOH)_2 \cdot 2H_2O$ via seed layers and through sol-gel process. The need for surfactant is fulfilled by the use of 2-methoxyethanol (ME) $CH_3OCH_2CH_2OH$. The stock solution for the samples was prepared by using different grams of Zinc acetate powder which equivalent in molar to (1.0 ,0.9 ,0.8 , 0.7 ,0.6 ,0.5 , 0.4 ,0.3 ,0.2 and 0.1 molar) as illustrated in table 3.1.

Table 3.1: shows the amounts of zinc acetate in molar used to synthesized ZnO nanostructures.

| | | | | | | | | | | |
|--|-----|-----|-----|-----|-----|-----|-----|-----|-----|-----|
| Sample number | 1 | 2 | 3 | 4 | 5 | 6 | 7 | 8 | 9 | 10 |
| Mass of Zinc acetate dehydrate in gram | 195 | 175 | 156 | 137 | 117 | 98 | 78 | 59 | 39 | 20 |
| Concentration of zinc acetate in molar (M) | 1.0 | 0.9 | 0.8 | 0.7 | 0.6 | 0.5 | 0.4 | 0.3 | 0.2 | 0.1 |

Then each molar of zinc acetate was dissolved in 100 ml of ethanol in glass beakers. After that, each solution was continuously stirred for 60 min at $80^\circ C$ to get a milky solution of a zinc acetate, Figure (3.1). Next step, some drops of 2-methoxyethanol (ME) was added carefully to the milky solution as stabilizer to obtain a homogeneous and transparent solution as seen in Figure(3.2).

Figure (3.1): shows a milky solution of Zinc Acetate for preparing the sample 3.



Figure (3.2) : Shows the as-obtained transparent solutions of the ten samples

Finally, the Zinc oxide solution has been got. The stirring of the mixture was continued for additional time around 30 min to complete the reaction for obtaining a gel-like product. Then the ten samples have been aged by put them in the laboratory at room temperature for 48 hours. After that the samples were washed by distilled water to obtain the final sol-gel products. The sol-gel for each sample was used to prepare the film by spinner (spin coating). The films were prepared using the indium -tin -oxide (ITO) as conducting coated glasses substrates. The slides were cleaned several times with ethanol and then were washed with deionizer water and acetone respectively. The coating films by ITO/glass were performed at room temperature using the centrifuge machine, with suitable speed rate for 60 s. Finally, the samples are ready for characterization.

3.2 Characterization Techniques and Instruments

The as-prepared zinc oxide nanostructures presented in this thesis was characterized in detail, in terms of their structural, morphological, compositional and optical properties. The crystal structures of the samples were characterized at room temperature by using a Philips PW1700 X-ray Diffractometer. The morphological properties of the synthesized zinc oxide nanomaterials were characterized by SEM technique. The locations of band position of the elements were examined by using the Fourier Transform Infrared Spectrophotometer (FTIR) in the range of 400 to 4000 cm^{-1}

to record some location of the band positions. The optical properties were examined by using UV-visible spectroscopy.

3.3 Structural Analysis

3.3.1 X-ray Diffraction Analysis

X-rays are electromagnetic radiation of wavelength about 1 \AA (10^{-10} m), which is about the same size as an atom. They occur in that portion of the electromagnetic spectrum between gamma-rays and the ultraviolet. The discovery of X-rays in 1895, is a non-destructive type of analytical technique which provides valuable insight about the lattice structure of a crystalline substance like unit cell dimensions, bond angles etc. XRD is based on the principle of constructive interference of x-rays and the sample concerned which should be crystalline.

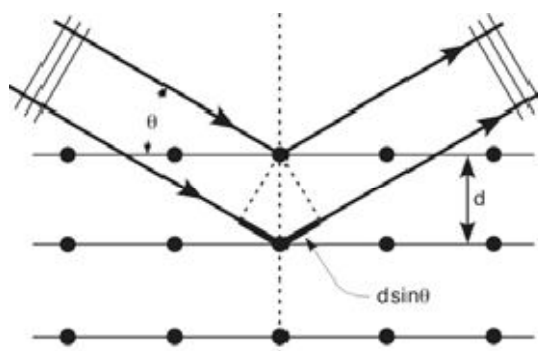


Figure (3.3): Reflection of x-rays from two planes of atoms in a solid.

Figure (3.3) illustrates the reflection of x-rays from two planes of atoms in a solid. A crystal lattice is a regular three-dimensional distribution (cubic, rhombic, etc.) of atoms in space. These are arranged so that they form a series of parallel planes separated from one another by a distance d , which varies according to the nature of the material. For any crystal, planes exist in a number of different orientations – each with its own specific d -spacing. When a monochromatic X-ray beam with wavelength λ is projected onto a crystalline material at an angle θ , diffraction occurs only when the distance traveled by the rays reflected from successive planes differs by a complete number n of wavelengths, which leads to famous Bragg's Law:

$$n\lambda=2d\sin(\theta)(3.1)$$

where n is an integer 1,2,3...(usually equal 1), λ is wavelength in angstroms (1.54 Å for copper), d is interatomic spacing in angstroms, and θ is the diffraction angle in degrees. By varying the angle theta, the Bragg's Law conditions are satisfied by different d-spacing in polycrystalline materials. Plotting the angular positions and intensities of the resultant diffracted peaks of radiation produces a pattern, which is characteristic of the sample. Where a mixture of different phases is present, the resultant diffract-gram is formed by addition of the individual patterns. Based on the principle of X-ray diffraction, a wealth of structural, physical and chemical information about the material investigated can be obtained.

The x-rays which are generated by a CRT are filtered, collimated and then directed towards the sample. The interaction that follows produces constructive interference based on Bragg's law which relates wavelength of the incident radiations to the diffraction angle and lattice spacing. The x-rays that are obtained on diffraction are counted after proper processing. By altering the various parameters like the geometry of incident rays and the orientation of the detector and crystal, we obtain all possible diffraction directions of the lattice [81, 82].

3.3.2 Fourier Transform Infrared Spectrophotometer (FTIR)

The physics of the individual atoms and simple molecules can be understood by studying their interaction with electromagnetic radiations. This study is called as spectroscopy. In spectroscopy, electromagnetic radiation of a particular frequency or a range of frequencies is allowed to fall on a sample under study. The radiation coming out of the sample is then analyzed in terms of the intensity at different frequencies. This indicates about the line absorbed or emitted by the molecule, and hence giving a picture of the molecular energy levels. In the region of longer wavelength or low frequency the identification of different types of chemicals is possible by the technique of infrared spectroscopy and the instrument requires for its execution is Fourier transform infrared (FTIR) spectrometer (Figure 3.4). The spectroscopy merely based on the fact that molecules absorb specific frequencies that are characteristic of their structure termed as

resonant frequencies, i.e. the frequency of the absorbed radiation matches the frequency of the bond or group that vibrates. And the detection of energy is done on the basis of shape of the molecular potential energy surfaces, the masses of the atoms, and the associated vibronic coupling. Sometimes help of approximation techniques like Born–Oppenheimer and harmonic approximations are also taken. As each different material is a unique combination of atoms, no two compounds produce the exact same infrared spectrum. Therefore, infrared spectroscopy can result in a positive identification (qualitative analysis) of every different kind of material. In addition, the size of the peaks in the spectrum is a direct indication of the amount of material present [83, 84]. FTIR can be used to analyze a wide range of materials in bulk or thin films, liquids, solids, pastes, powders, fibers, and other forms. FTIR analysis can give not only qualitative (identification) analysis of materials, but with relevant standards, can be used for quantitative (amount) analysis. FTIR can be used to analyze samples up to ~11 millimeters in diameter, and either measure in bulk or the top ~1 micrometer layer. FTIR spectra of pure compounds are generally so unique that they are like a molecular "fingerprint".



Figure(3.4): shows the Fourier transform Infrared Spectroscopy
https://en.wikipedia.org/wiki/Fourier-transform_infrared_spectroscopy

3.3.3 Surface and Morphological Analysis

3.3.3.1 Scanning Electron Microscope

The scanning electron microscope (SEM) is a type of electron microscope that

image the sample surface by scanning it with a high-energy beam of electrons in a raster scan pattern. The electrons interact with the atoms to make the sample producing signals that contain information about the sample's surface topography, composition and other properties such as electrical conductivity. The types of signals produced by an SEM include secondary electrons; back scattered electrons (BSE), characteristic x-rays, light (cathodoluminescence), specimen current and transmitted electrons. These types of signal all require specialized detectors for their detection that are not usually all present on a single machine.

The schematic image of SEM is illustrated in Figure (3.5a and b), in order to show how it works. The SEM uses electrons instead of light to form an image. A beam of electrons is produced at the top of the microscope by heating of a metallic filament. The electron beam follows a vertical path through the column of the microscope. It makes its way through electromagnetic lenses which focus and direct the beam downwards towards the sample. Once it hits the sample, other electrons such as backscattered or secondary are ejected from the sample. Detectors collect the secondary or backscattered electrons, and convert them to a signal that is sent to a viewing screen similar to the one in an ordinary television, producing an image [85,86]. The SEM has a large depth of field, which allows a large amount of the sample to be in focus at one time. The SEM also produces images of high resolution, which means that closely spaced features can be examined at high magnification (up to $\times 300000$) as compared to light microscopy (up to $\times 10000$). But as the images are created without light waves, they are black and white. The combination of higher magnification, larger depth of focus, greater resolution, and ease of sample observation makes the SEM one of the most heavily used instruments in research areas today.

To characterize the morphology and the surface of the as-grown ZnO nanostructures, the ten samples were sent to China for scanning electron microscope (SEM).

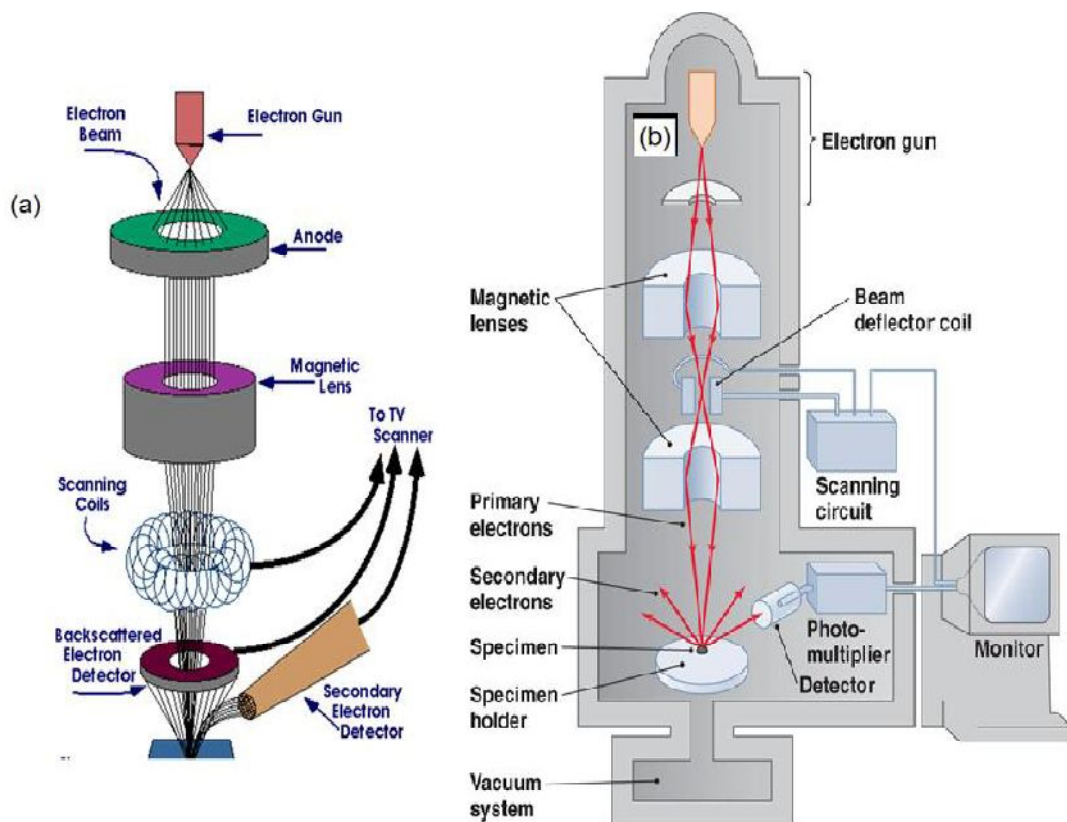


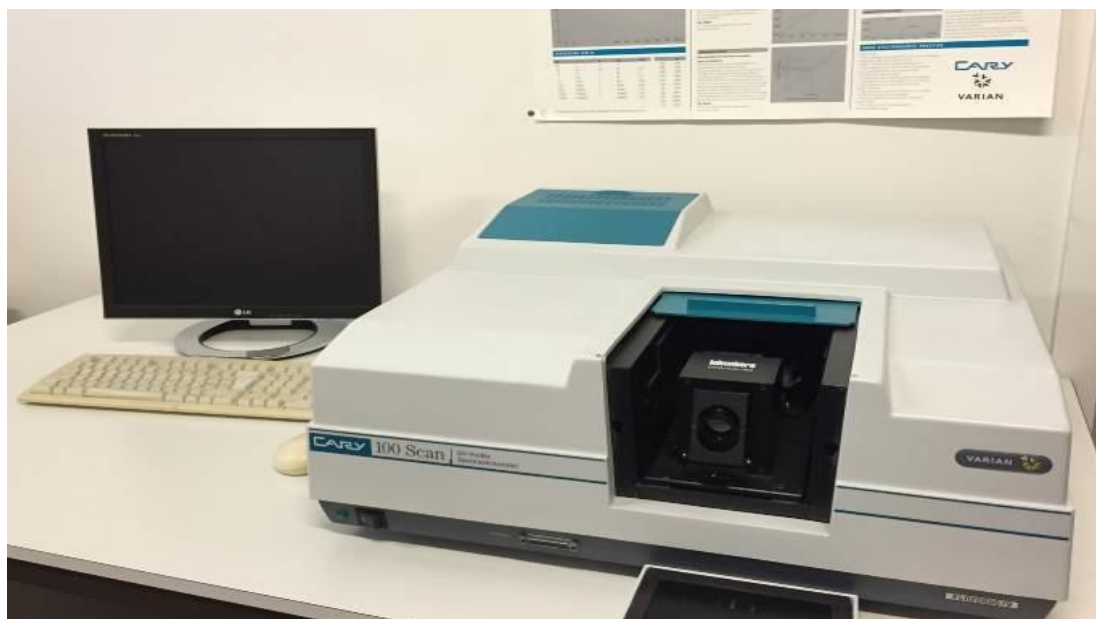
Figure (3.5): (a) and (b) show schematics diagram for Scanning Electron Microscope (SEM).
<https://www.purdue.edu/epps/rem/rs/sem.htm>

The SEM gives information on the morphology of the surface of the samples, which implies that it is possible to determine if any growth has taken place. However, the images from the SEM are not a definitive proof that the obtained nanostructures actually consist of ZnO. Even though the SEM produces 3D images, they give no information regarding the exact atomic structure of the sample. The 3D images are easy to interpret and they reveal topographic features of the sample. The SEM images allow us to examine the diameter, length, shape and density of the ZnO nanostructures.

3.3.4 UV-Visible Spectroscopy

Ultraviolet and visible spectrometers have been used for the last several years and over this period have become the most important analytical instrument in the modern day laboratory. In many applications other techniques could be employed but none rival UV-

Visible spectrometry for its simplicity, versatility, speed, accuracy and cost-effectiveness. The structures of the compounds prepared in the lab are verified by spectroscopic techniques. UV Vis spectrometer is a tool used for the investigation of electronic transitions and hence to determine the electronic bonding in a molecule. In Ultraviolet/Visible (UV-Vis) spectroscopy, electromagnetic radiation is emitted within the wavelength range of about 200 to 800 nm from the source. The source is often a Deuterium (or hydrogen) lamp, a tungsten filament lamp, or a xenon arc lamp. The radiation from the source is then passed through a wavelength selector (either a diffraction grating or filter) through which a narrow band of wavelengths can pass. In a standard UV-Vis spectrometer, the beam of light is split into two parts by a partial mirror; one half of the beam (the sample beam) is directed through a transparent cell containing a solution of the compound being analyzed, and one half (the reference beam) is directed through an identical cell that does not contain the compound but contains the same solvent wherein the compound is dissolved. The beam from the wavelength selector passes through the sample and is absorbed by the sample according to Beer's law. The difference of light intensities scanned over a range of wavelength are taken and compared. The intensity profiles over a range of wavelengths are observed. In complex molecules the energy levels are more closely spaced and photons of near ultraviolet and visible light can affect the transition. These substances, therefore, will absorb light in some areas of the near ultraviolet and visible regions. In this study the UV-Vis. spectroscopy was used to examine the optical properties of as-prepared zinc oxide nanomaterials. Figure 2.9 exhibits a picture of UV-Visible spectrophotometer.



Figure(3.6): shows the Ultraviolet/Visible (Uv vis) spectroscopy.
https://www.researchgate.net/figure/17-Spectrophotometre-UV-Vis-VARIAN-Cary-100-Scan_fig16_278826646

Chapter Four

Results and Discussion

4.1 Introduction

Nanostructures have attracted attention of researchers for their many important technological applications. The synthesis of nanostructures is a budding area of research. Also, the synthesis of nanostructures by a low cost process would be of great technological importance. Chapter 4 describes the main results and the discussion of the thesis. The ZnO films/nanocomposites received in this study were synthesized by using sol-gel method. The study has used different concentrations of zinc acetate in order to see whether it can make change in the morphology of ZnO that formed on TIO glass, also to investigate the effect of these concentrations on the optical properties of the synthesized ZnO nanostructures.

4.2 Crystal Structure and Morphology

Detailed characterizations in terms of crystallite structures and morphology using standard techniques are presented by using X-ray diffractometer, Scanning Electron Microscopy (SEM) and Fourier Transform Infrared Spectrophotometer (FTIR).

4.2.1 X-ray Diffraction Analysis

The study used the Philips PW1700 X-ray diffractometer in order to investigate the crystal structure of as-synthesized samples of ZnO nanostructures. It operated at voltage of 40 kV and current of 30 mA. The samples were scanned between 0° and 120° at a scanning speed of 0.06°C/s using Cu $K\alpha$ radiation with $\lambda = 1.5418\text{\AA}$. The X-ray diffraction pattern of the synthesized ZnO 1.0 M nanocrystals has been shown in Fig (4.1). The characteristic diffraction peaks of ZnO 1.0 M nanocrystals are appeared at 2-theta values of 33.5027° , 38.8780° , 56.1542° , 70.4007° , 83.4586° , 92.9933° and 96.177° , corresponding to crystalline diffraction planes of (111), (200), (220), (222), (400), (331), and (420) respectively. The XRD patterns indicates that the ZnO 1.0 M nanostructures is a local cubic structure. Also the XRD data Table (4.1) established that all samples of as-

synthesized ZnO films nanostructures, the d-spacing decreases with increasing the values of 2 theta (2θ) in agreement with Bragg's law. Table (4.2), shows other parameters of ZnO 1.0 M nanocrystals at various crystalline orientations which confirmed that the cubic structures of as-synthesized ZnO 1.0 M has lattice constant $a = b = c = 8.3981 \text{ \AA}$ [96] and density of 5.4495 g/cm^3 in agreement with standard value 5.6 g/cm^3 table 2.1.

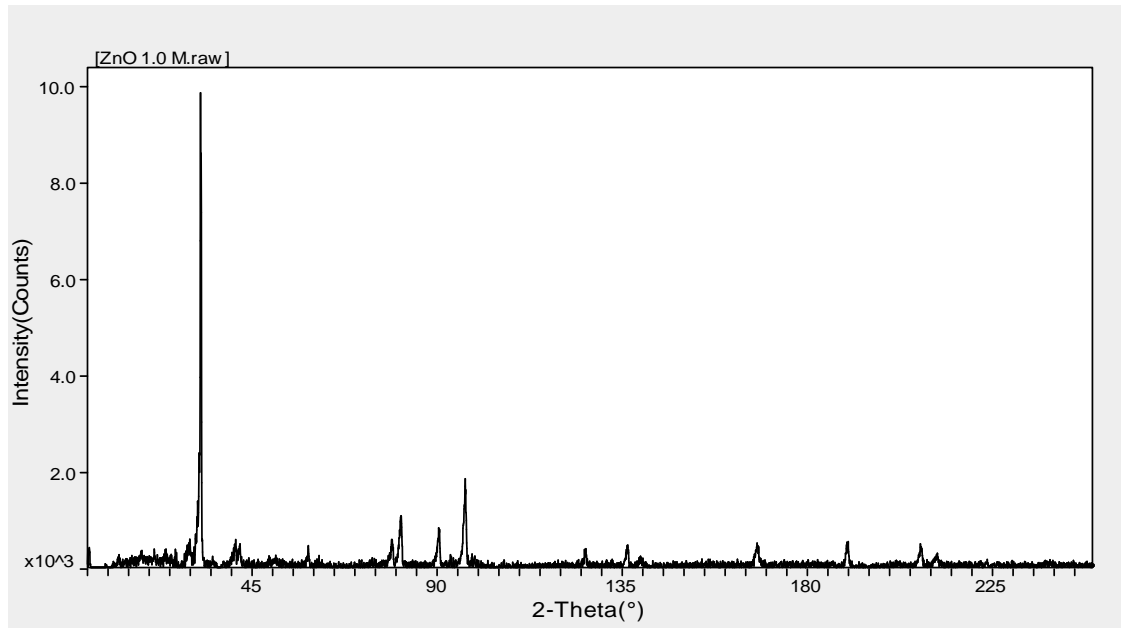


Figure (4.1): The XRD patterns of the as-synthesized ZnO nanostructures for sample 1.0 M.

Figure (4.2) shows the X-ray diffraction patterns of the synthesized sample ZnO 0.9 M nanocrystals. The diffraction peaks of sample ZnO 0.9 M nanostructures are appeared at 2-theta values of 33.5027° , 38.8780° , 56.1542° , 70.4007° , 83.4586° , 92.9933° and 96.177° , corresponding to crystalline diffraction planes of (111), (200), (220), (222), (400), (331), and (420) respectively. These results confirm that the as-synthesized ZnO 0.9 M nanostructures crystallized at local cubic structure with lattice constant $a = b = c = 8.3981 \text{ \AA}$ [96]. Table 4.1 proved that the d-spacing decreases with increasing the values of 2 theta. Table 4.2, shows other parameters of XRD pattern of the sample ZnO 0.9 M nanocrystals at various crystalline orientations. Also Table 4.2 indicates that the as-synthesized ZnO has density of 5.4494 g/cm^3 in agreement with standard value.

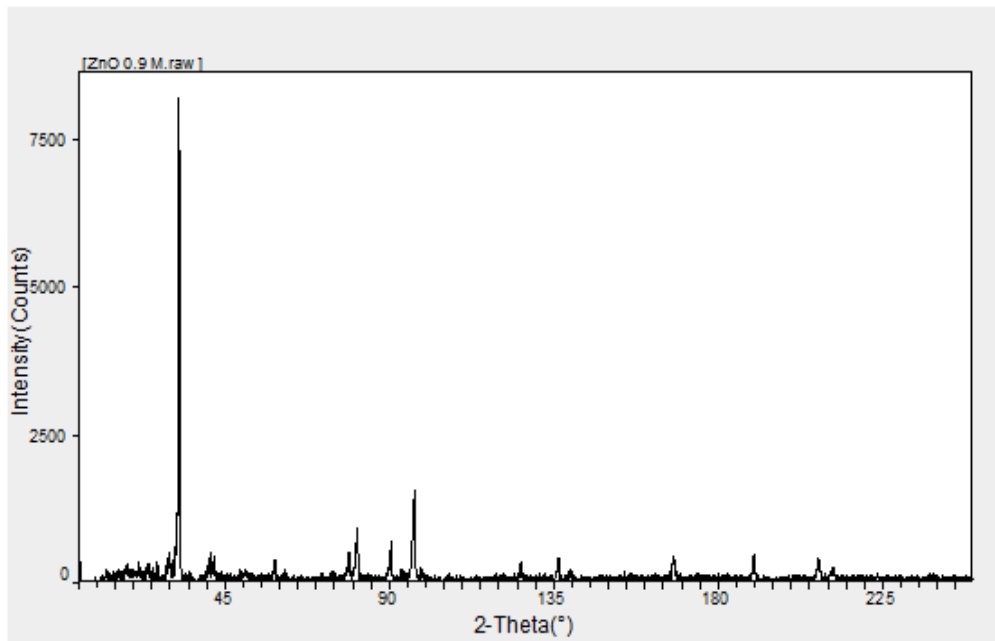


Figure (4.2): The XRD patterns of the as-synthesised ZnO sample 0.9 M nanostructures

Figure (4.3) shows the X-ray diffraction patterns of the synthesized sample ZnO 0.8 M nanocrystals. The diffraction peaks of ZnO 0.8 M nanostructures are also visible at 2-theta values of 33.5027° , 38.8780° , 56.1542° , 70.4007° , 83.4586° , 92.9933° and 96.177° , corresponding to crystalline diffraction planes of (111), (200), (220), (222), (400), (331), and (420) respectively. These results confirm that the as-synthesized ZnO 0.8 M nanostructures is a local cubic structure with lattice constant $a = b = c = 8.3981 \text{ \AA}$ [96]. Table 4.1, proved that the d-spacing decreases with increasing the values of 2 theta. Table 4.2, shows other parameters of XRD pattern of ZnO 0.8 M nanocrystals at various crystalline orientations, which shows the as-synthesized ZnO has density of 5.4493 g/cm^3 .

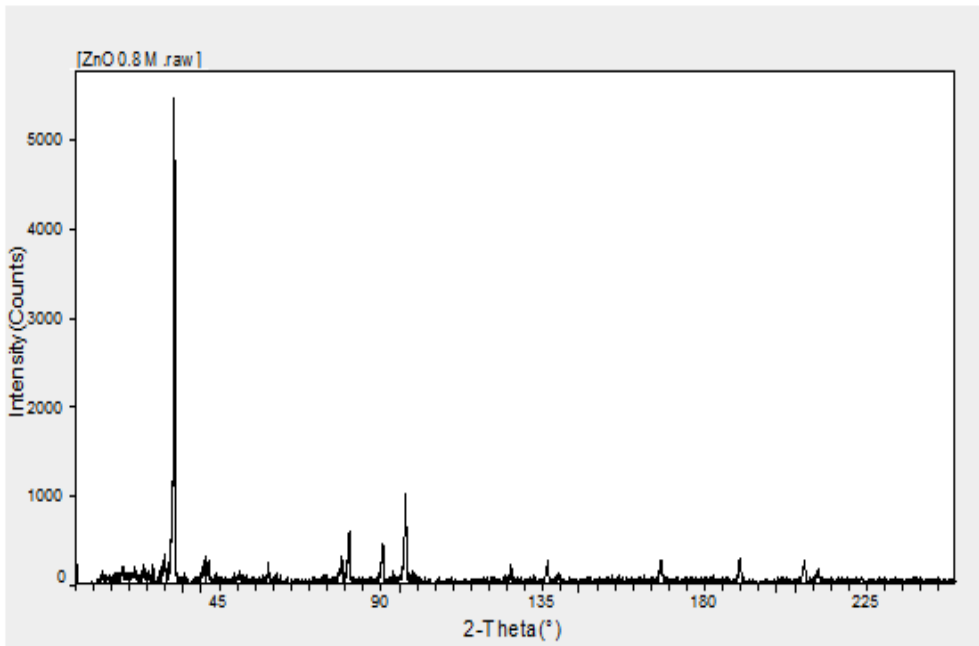
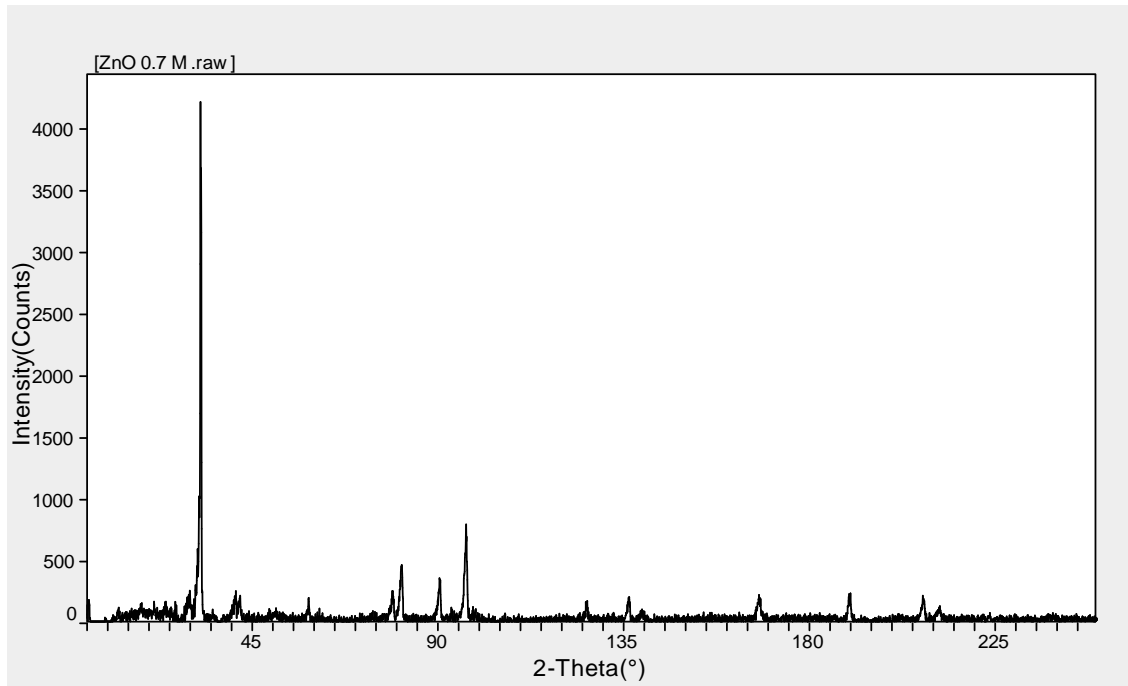


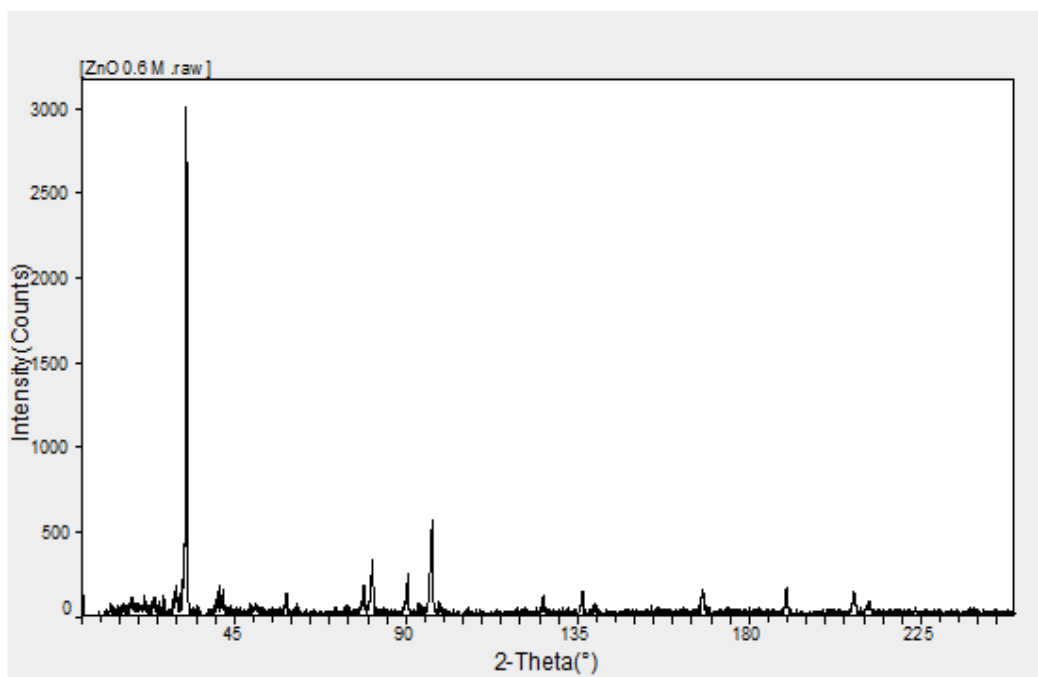
Figure (4.3): The XRD patterns of the as- synthesised ZnO sample 0.8 M nanostructures

Figure (4.4) demonstrates the X-ray diffraction patterns of the synthesized ZnO 0.7 M nanocrystals. The diffraction peaks of ZnO 0.7 M nanostructures are appeared at 2-theta values of 33.5027° , 38.8780° , 56.1542° , 70.4007° , 83.4586° , 92.9933° and 96.177° , corresponding to crystalline diffraction planes of (111), (200), (220), (222), (400), (331), and (420) respectively. The sharp peak at 2Θ of 33.5027° has highest intensity of about 4500 a.u. These results corroborated that the as-synthesized ZnO 0.7 M nanostructures is local cubic structure with lattice constant $a = b = c = 8.3981 \text{ \AA}$ [96]. The recorded data in table 4.1, proved that the d-spacing decreases with increasing the values of 2 theta. Table 4.2, represents other parameters of XRD pattern of ZnO 0.7 M nanocrystals at various crystalline orientations, in which shows that the as-synthesized ZnO has density of 5.4492 g/cm^3 .



Figure(4.4): The XRD patterns of the as- synthesised ZnO sample 0.7 M nanostructures

Figure(4.5) represents X-ray diffraction patterns of the synthesized ZnO 0.6 M nanostructures. As can be seen, the diffraction peaks of sample ZnO 0.6 M nanostructures are became visible at 2-theta values of 33.5027° , 38.8780° , 56.1542° , 70.4007° , 83.4586° , 92.9933° and 96.177° , which corresponding to crystalline diffraction planes of (111), (200), (220), (222), (400), (331), and (420) respectively. These results established that the as-synthesized sample of ZnO 0.6 M nanostructures is a local cubic structure with lattice constant $a = b = c = 8.3981 \text{ \AA}$ [96]. The recorded data in table 4.1 proved that the d-spacing decreases with increasing the values of 2 theta. Table 4.2, shows other parameters of XRD pattern of ZnO 0.6 M nanocrystals at various crystalline orientations, in which the as-synthesized ZnO has density of 5.4491 g/cm^3 .



Figure(4.5): The XRD patterns of the as- synthesised sample ZnO 0.6 M nanostructures.

Figure (4.6) shows the X-ray diffraction patterns of the synthesized ZnO 0.5 M nanocrystals. The diffraction peaks of the sample ZnO 0.5 M nanostructures are materialized at 2-theta values of 33.5027° , 38.8780° , 56.1542° , 70.4007° , 83.4586° , 92.9933° and 96.177° , corresponding to crystalline diffraction planes of (111), (200), (220), (222), (400), (331), and (420) respectively. This pattern confirm that the as-synthesized ZnO 0.5 M nanostructures showed a local cubic structure with lattice constant $a = b = c = 8.3981 \text{ \AA}$ [96]. Also, the pattern revealed the peak at 2θ 33.5027° shows the highest intensity at about 2400 (a.u) for this sample. Table (4.1) characterized the d-spacing distances according to diffraction peaks and proved that it decreases with increasing the values of 2 theta. Table (4.2), shows other XRD parameters of sample ZnO 0.5 M nanocrystals at various crystalline orientations. Table 4.2 shows the as-synthesized ZnO has density of 5.4490 g/cm^3 .

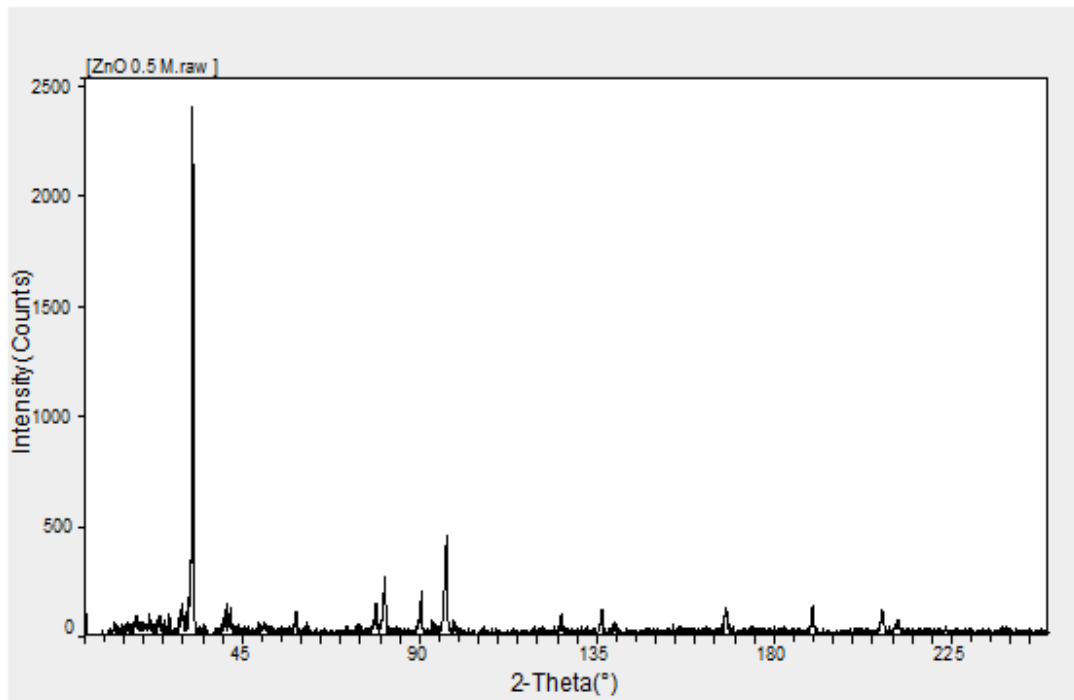


Figure (4.6): The XRD patterns of the as- synthesised ZnO sample 0.5 M nanostructures.

Figure(4.7) shows the X-ray diffraction patterns of the synthesized of ZnO 0.4 M nanocrystals. The diffraction peaks of ZnO 0.4 M nanostructures are appeared at 2-theta values of 33.5027° , 38.8780° , 56.1542° , 70.4007° , 83.4586° , 92.9933° and 96.177° , which corresponding to crystalline diffraction planes of (111), (200), (220), (222), (400), (331), and (420) respectively. These results verified that the as-synthesized ZnO 0.4 M nanostructures is a local cubic structure with lattice constant $a = b = c = 8.3981 \text{ \AA}$ [96]. Also, the pattern revealed the peak at $2\theta 33.5027^\circ$ shows the highest intensity at about 2200 (a.u) for ZnO 0.4 M sample. The recorded data in table 4.1, proved that the d-spacing decreases with increasing the values of 2 theta, in agreement with Bragg's law. Table (4.2), shows other XRD parameters of ZnO 0.4 M nanocrystals at various crystalline orientations. Table 4.2, shows the cubic structures has a density of 5.4489 g/cm^3 .

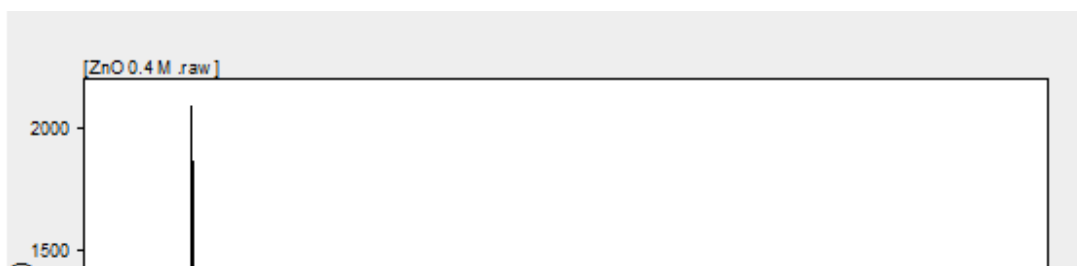
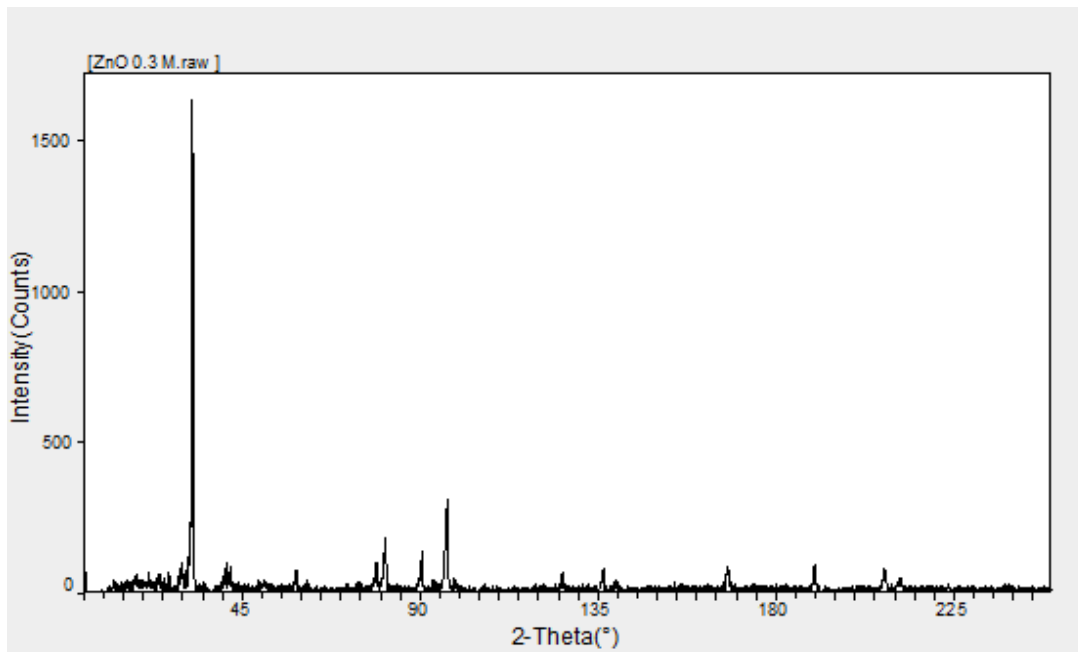


Figure (4.7): The XRD patterns of the as-synthesised ZnO sample 0.4 M nanostructures

Figure (4.8) shows the X-ray diffraction patterns of the synthesized ZnO 0.3 M nanocrystals. The diffraction peaks of ZnO 0.3 M nanostructures are appeared at 2-theta values of 33.5027° , 38.8780° , 56.1542° , 70.4007° , 83.4586° , 92.9933° and 96.177° , corresponding to crystalline diffraction planes of (111), (200), (220), (222), (400), (331), and (420) respectively. These results revealed that the as-synthesized ZnO 0.3 M nanostructure is a local cubic structure with lattice constant $a = b = c = 8.3981 \text{ \AA}$ [96], in agreement with the theoretical values. Also, the pattern showed the peak at $2\Theta = 33.5027^\circ$ has the highest intensity at about 1800 (a.u) for sample ZnO 0.3 M. The recorded data in table 4.1, proved that the d-spacing decreases with increasing the values of 2 theta in agreement with Bragg's law. Table 4.2, shows other parameters of XRD pattern of ZnO 0.3 M nanocrystals at various crystalline orientations in which, the as-synthesized ZnO has a density of 5.4488 g/cm^3 .



Figure(4.8): shows the X-ray diffraction patterns of the synthesized ZnO 0.2 M nanostructures. The diffraction peaks of ZnO 0.2 M nanostructures are appeared at 2-theta values of 33.5027° , 38.8780° , 56.1542° , 70.4007° , 83.4586° , 92.9933° and 96.177° , matched to crystalline diffraction planes of (111), (200), (220), (222), (400), (331), and (420) respectively. These results confirm that the as-synthesized ZnO 0.2 M films nanostructures is a local cubic structure with lattice constant of $a = b = c = 8.3981 \text{ \AA}$ [96]. Also, the pattern showed the peak at $2\Theta 33.5027^\circ$ has the highest intensity at about 1400 (a.u) for ZnO 0.2 M sample. The recorded data in table 4.1, proved that the d-spacing decreases with increasing the values of 2 theta, in agreement with Bragg's law. Table 4.2, shows other parameters of XRD pattern of ZnO 0.2 M nanocrystals at various crystalline orientations. Table 4.2, shows the as-synthesized ZnO has a density of 5.4487 g/cm^3 .

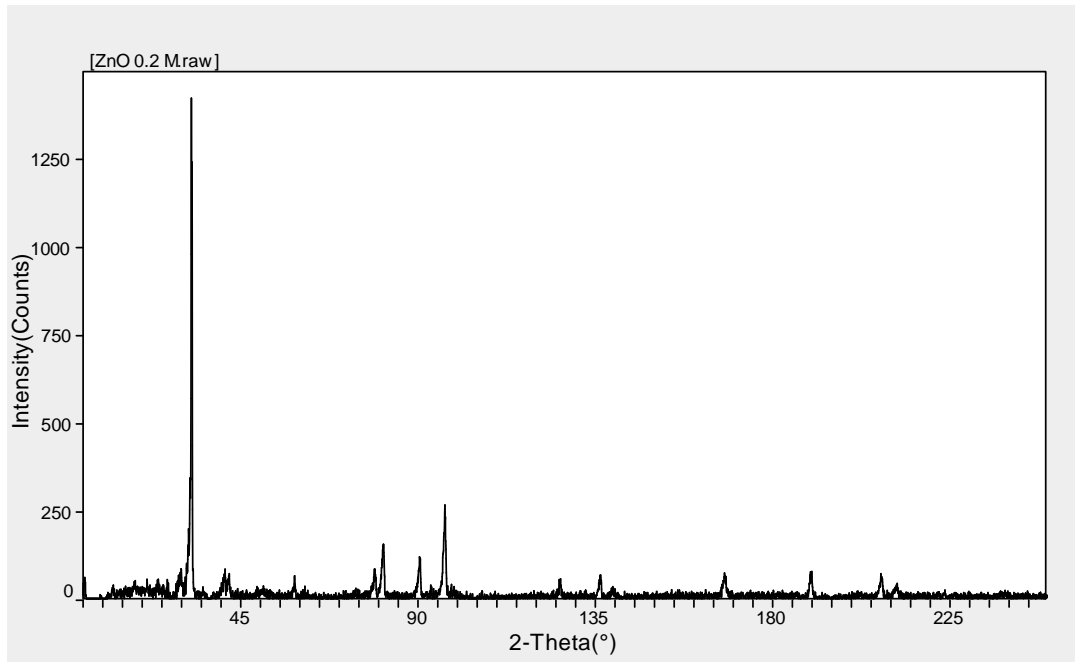
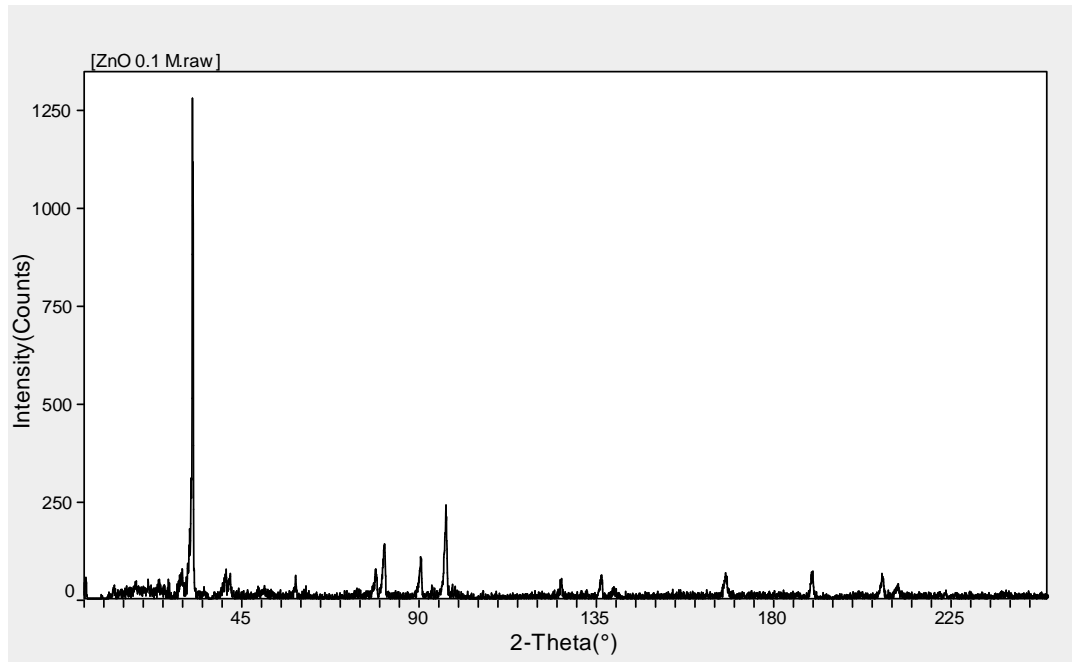


Figure (4.9): The XRD patterns of the as-synthesised ZnO sample 0.2 M nanostructures.

Figure (4.10) shows the X-ray diffraction patterns of the synthesized ZnO 0.1 M nanocrystals. The diffraction peaks of ZnO 0.1 M nanostructures became visible at 2-theta values of 33.5027° , 38.8780° , 56.1542° , 70.4007° , 83.4586° , 92.9933° and 96.177° , corresponding to crystalline diffraction planes of (111), (200), (220), (222), (400), (331), and (420) respectively. These results revealed that the as-synthesized ZnO 0.1 M nanostructures is local cubic structure with lattice constant of $a = b = c = 8.3981 \text{ \AA}$ [96]. Also, the pattern of sample 0.1 M illustrated the peak at $2\Theta 33.5027^\circ$ has the highest intensity at about 1300 a.u. The recorded data in table 4.1, proved that the d-spacing decreases with increasing the values of 2 theta in agreement with Bragg's law. Table 4.2, shows other parameters of XRD pattern of ZnO 0.1M nanocrystals at various crystalline orientations in which, the as-synthesized ZnO nanostructures has a density of 5.4486 g/cm^3 .



Fig(4.10): The XRD patterns of the as- synthesised ZnO 0.1 M samplenanostructures

Figure(4.11) represents the XRD patterns of all synthesized ZnOnanostructures samples denoted as 1.0, 0.9, 0.8, 0.7, 0.6, 0.5, 0.4,.0.3,.0.2 and 0.1 molars. These molars indicate the concentrations of zinc acetate using during synthesizing the ZnO nanocrystals respectively. The XRD patternsfor all samples received in this study showed there is a sharp peak at $2\Theta = 33.5027^\circ$ corresponding to (111) plane. Interestingly, among the all samples, the highest intensity is found to be about 9950 (a.u) for sampleZnO 1.0 M at the sharp peak of $2\Theta = 33.5027^\circ$ which indicated that the crystallinity of the as-synthesized ZnO films samples increase with increasing the concentrations of zinc acetate. Also, this sharp peak indicates that the particles have grown and the crystal quality has been improved when increasing the concentration of zinc acetate. Moreover, any other additional impurity peaks are not detected in the XRD patterns, which imply the high purity of synthesized ZnO nanostructures obtained in this study. Interestingly, the crystal structure of as –synthesizedZnOin this study produced a local cubic structure which differed from the majority recent publishing papers which reported the most commonly structure of hexagonal wurtzitestructures. Taking into account, the cubic ZnOstructure is

metastable and can be stabilized only by growth on cubic substrates such as Pt/Ti/SiO₂/Si [87] and indium-tin-oxide (ITO) slides glasses, reflecting topological compatibility to overcome the intrinsic tendency of forming wurtzite phase [88, 89]. This study used indium-tin-oxide (ITO) slides glass as conducting substrates as well as to enhance the growth of as-synthesized ZnO nanostructures. Hexagonal and zinc blende cubic structures don't display inversion symmetry and it is properties like these that are responsible for the piezoelectricity and pyroelectricity of ZnO [90].

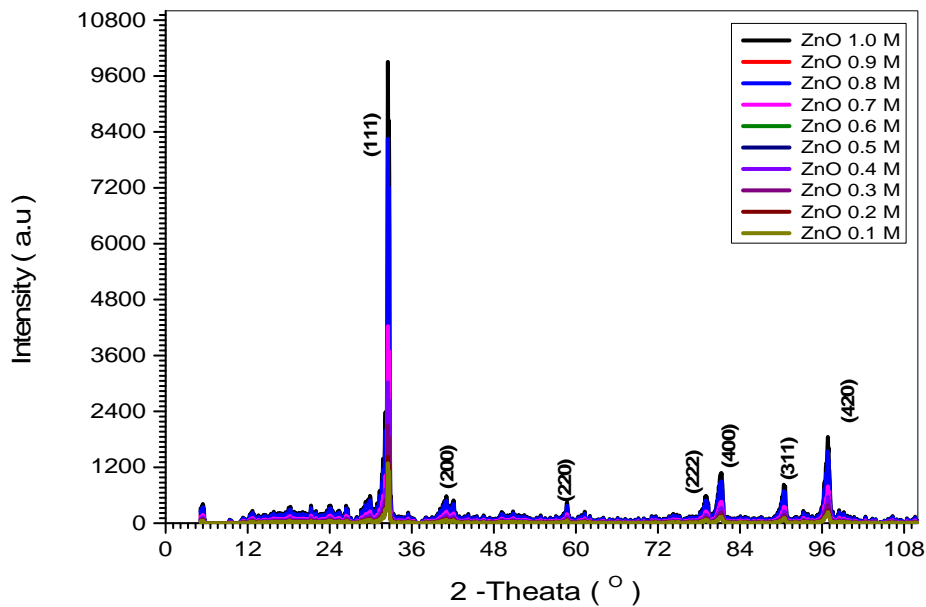


Figure (4.11): represents the XRD charts of the ten samples of as-synthesized ZnO nanostructures using different concentrations of zinc acetate.

Table 4.1, represents the d-spacing distances between crystal planes in the cubic structure of as-synthesized ZnO nanostructures according to diffraction peaks of (111), (200), (220), (222), (400), (311), and (420) respectively. The d-spacing distances have been calculated by using the equation [94].

$$\frac{1}{d^2} = \frac{h^2 + k^2 + l^2}{a^2} \quad (4.1)$$

a is the lattice parameter of each structure, and h , k , and l are the Miller-Bravais-indices of the crystal plane. From the table4.1,the results illustrated that the inter planner d-spacing distances decrease with increasing the values of 2θ which obey Bragg's law $n\lambda = 2d \sin\theta$.

Table4.1: shows the parameters of 2-Theta, Miller indices and d – spacing of the ten samples of ZnO respectively.

| 2-Theta | h | k | l | d (Å) |
|---------|---|---|---|---------|
| 33.5027 | 1 | 1 | 1 | 2.67255 |
| 38.8784 | 2 | 0 | 0 | 2.31450 |
| 56.1542 | 2 | 2 | 0 | 1.63660 |
| 78.4007 | 2 | 2 | 2 | 1.33628 |
| 83.4586 | 4 | 0 | 0 | 1.15725 |
| 92.9933 | 3 | 3 | 1 | 1.06197 |
| 96.1770 | 4 | 2 | 0 | 1.03508 |

Table 4.2, shows other XRD parameters of as –synthesized ZnO nanocrystals at various crystalline orientations. These parameters are crystal form, lattice parameters (a,b,c , β,α , γ), the density, particle size, d – spacing and average lattice. As can be observed, the unit cell confirmed the as-synthesized ZnO films nanostructure are local cubic structure. Also can be seen that the crystal size for ZnO 1.0 M sample is 20.10 nm where for ZnO 0.1 M sample is 145.23 nm, this results established the sizes of the nanostructures decreased with increasing the concentrations of zinc acetate and this may attributed to the well growth of the crystal at high concentrations.

Table 4.2: shows some crystallite lattice parameters of all samples of as-synthesized ZnO nanostructures.

| Sample | Structure | a=b=c(Å) | $\alpha = \beta = \gamma$ (°) | Density (g/cm ³) | Size(nm) | d-spacing(Å) | Average L-C |
|-----------|-----------|----------|-------------------------------|------------------------------|----------|--------------|-------------|
| ZnO 1.0 M | Cubic | 8.3981 | 90 | 5.4495 | 20.10 | 2.1433 | 25.4 |
| ZnO 0.9 M | Cubic | 8.3981 | 90 | 5.4494 | 26.93 | 2.1532 | 26.03 |
| ZnO 0.8 M | Cubic | 8.3981 | 90 | 5.4493 | 23.28 | 2.1548 | 27.68 |
| ZnO 0.7 M | Cubic | 8.3981 | 90 | 5.4492 | 24.25 | 2.1587 | 29.11 |
| ZnO 0.6 M | Cubic | 8.3981 | 90 | 5.4491 | 68.47 | 2.1608 | 29.21 |
| ZnO 0.5 M | Cubic | 8.3981 | 90 | 5.4490 | 92.15 | 2.1623 | 30.66 |
| ZnO 0.4 M | Cubic | 8.3981 | 90 | 5.4489 | 108.55 | 2.1654 | 36.75 |
| ZnO 0.3 M | Cubic | 8.3981 | 90 | 5.4488 | 114.83 | 2.1672 | 38.41 |
| ZnO 0.2 M | Cubic | 8.3981 | 90 | 5.4487 | 129.53 | 2.1687 | 39.34 |
| ZnO 0.1 M | Cubic | 8.3981 | 90 | 5.4486 | 145.23 | 2.1697 | 39.35 |

4.2.2 The relation between the concentrations and : dislocation density, crystal size, d-spacing and average lattice constant.

The dislocation density (δ) and number of unit cells of ZnOnanostructures in different concentrations are calculated and listed in table 4.2. The density (δ) of ZnOnanostructures is slightly increase with decreasing the concentration of zinc acetate by rate $10^{-3}(\text{g}\cdot\text{cm}^{-3}) \text{ mol}^{-1}$ as show in Figure (4.12). The result explained that the decreasing of δ at higher concentration of zinc acetate it leads to improve the crystal growth of ZnO ratio nanoparticles and also increase the proportion of surface atoms.

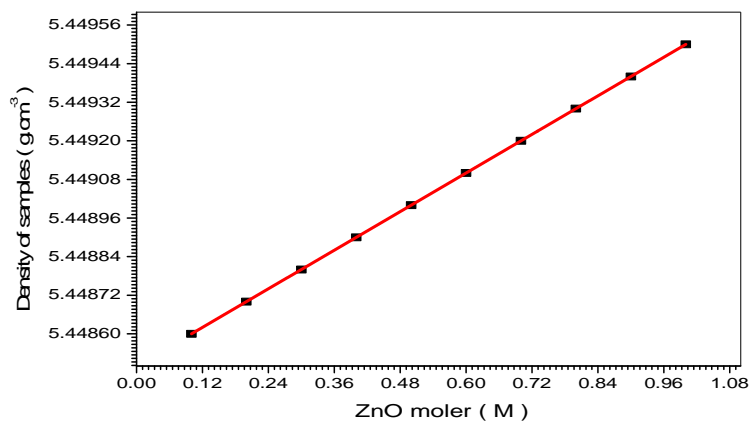


Figure (4.12):The relation between the Density and the concentrations of Ten samples of as-synthesized ZnO nanostructures.

Figure (4.13) is a plot graph showing the effect of the concentrations of zinc acetate (in molar) on the crystallite sizes obtained for as-synthesized ZnO nanostructures. The Figure(4.13), clearly demonstrates that the crystals sizes of ZnO nanostructures decreased when increasing the concentrations of zinc acetate. The decreasing in crystallite size is attributed to the high crystalline in the early stage at high concentrations .

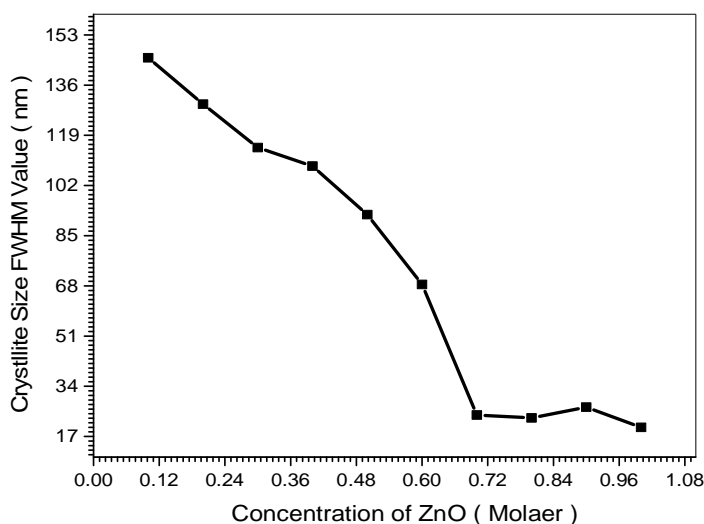


Figure (4.13) The relation between Crystallite size and the concentrations of zinc acetate for the ten samples of as-synthesized ZnO nanostructures.

Figure (4.14) shows the relation between the as-synthesized ZnO nanostructures and d-spacing for the samples. It can be seen that, the d-spacing of the ZnO nanostructures decrease with increasing the concentration of zinc acetate due to larger clusters. The d-spacing decreases with increasing the concentration by rate $(0.026 \text{ \AA} \cdot \text{mol}^{-1})$. The decreasing of d-spacing at low concentration, it may relate to prevent rapid growth of the crystals.

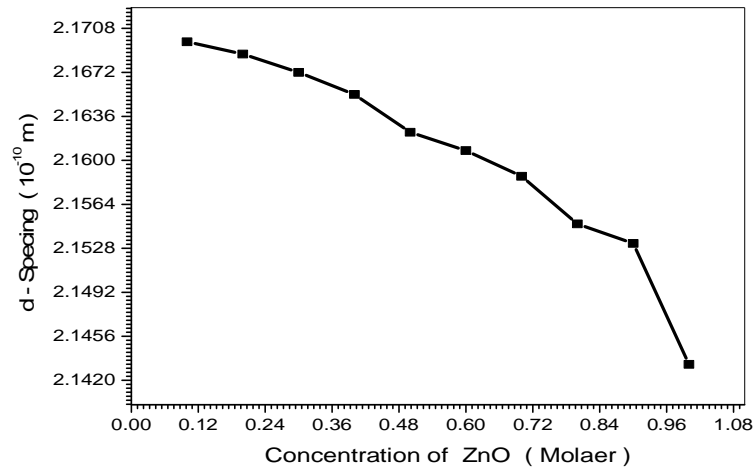
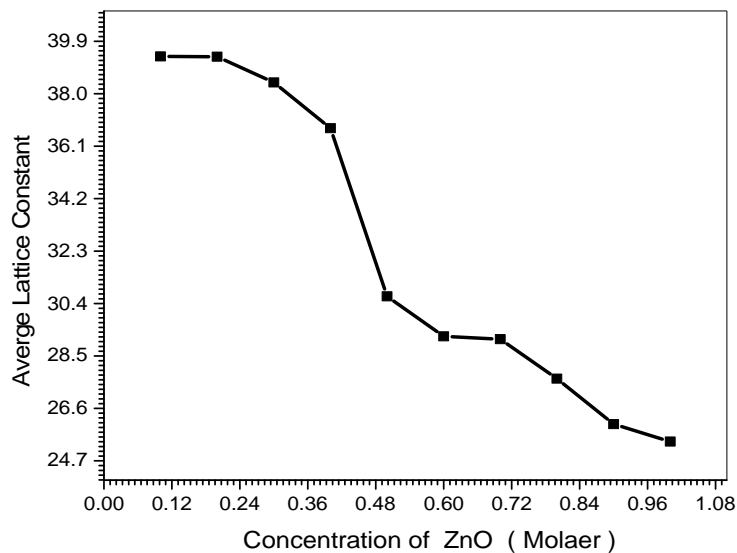


Figure (4.14):The relation between d- Spacing and concentrations of zinc acetate for the ten samples of as-synthesized ZnO nanostructures.

Figure (4.15) shows the relation between the Average Lattice Constant and the concentrations of zinc acetate to synthesize ZnO nanostructures. As can be seen that the average lattice constant decrease when increasing the concentrations of zinc acetate by rate (17.98 mol^{-1}).



Figure(4.15)The relation between Average Lattice Constant and concentration of zinc acetate for the ten samples of as-synthesized ZnO nanostructures.

4.3 Scanning Electron Microscopy (SEM) Analysis of ZnO samples

Figures 4.16 to 4.20 show the top-view SEM images of the synthesized ZnO film nanostructures grown on ITO/glass substrates. The as-synthesized ZnO film nanostructures were produced by using different concentrations of zinc acetate in molarities 1.0, 0.9, 0.8, 0.7, 0.6, 0.5, 0.4, 0.3, 0.2 and 0.1 respectively. The shape and the morphology of nanostructures in this study were analyzed using the Scanning Electron Microscope (SEM, Tuscan Vega LMU). The SEM image of ZnO 1.0 M film concentrations are shown in Fig (4.16). The high magnification image of sample 1.0 M indicates that like-date nanostructures of ZnO can be obtained by using the concentration of 1.0 molar. The like-date nanostructures for this sample (1.0 mol) are uniform in both morphology and particle size. Also, these like-date nanostructures are agglomerated and gathering together in different quantities. The average size was calculated to be 11.77 nm from the measurements on the SEM micrographs. This result is not close to the average crystallite size 20.1 nm calculated from XRD data, the difference may be attributed to that the size of nanostructure represented in SEM image was taken from a region containing nanoparticles with different sizes. Also, Figure 4.16 shows the SEM micrograph of sample ZnO 0.9 M using zinc acetate of concentration 0.9 mol. The result presents like-date nanostructures of ZnO 0.9 M which agglomerated together with uniform surface. The average size of these like-date nanostructures was estimated from the SEM graph and found to be 16.03 nm comparing to average size of 26.93 nm of ZnO 0.9 M sample calculated using the XRD data table (4.2). This may be attributed to that the result of SEM has been taken from a region that has different sizes of particles that agglomerated together.

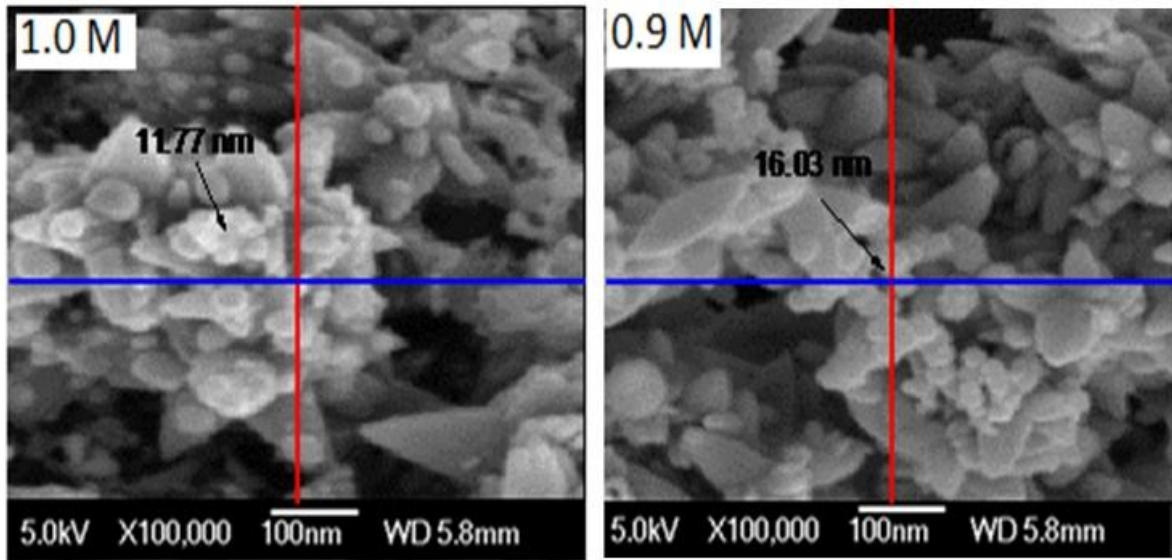


Figure (4.16): shows the SEM images for samples 1.0 M and 0.9 M respectively.

The SEM image of sample ZnO 0.8 M nanostructures are shown in Fig (4.17). The morphology in Figure (4.17, 0.8 M) indicates the as-synthesized of ZnO 0.8 M shows like-datenanostrctures. Thislike-datenanostructures of synthesized ZnO (0.8 mol) are agglomerated together in uniform shape. The mean particle size was estimated from SEM is equal to 18.63 nm close to that calculated from XRD data 23.28 nm. Figure (4.17, 0.7 M) shows a low magnification image of ZnO 0.7 M sample using zinc acetate of concentration 0.7 mol. It can be easily seen that the nanostrutures are closely packed together in a large amountwith uniform surface. The average size of these nanoparticles/nanostructures was estimated from the SEM graph and found to be 22.11 nm comparing to average size of 24.25 nm calculated using the XRD data table (4.2).

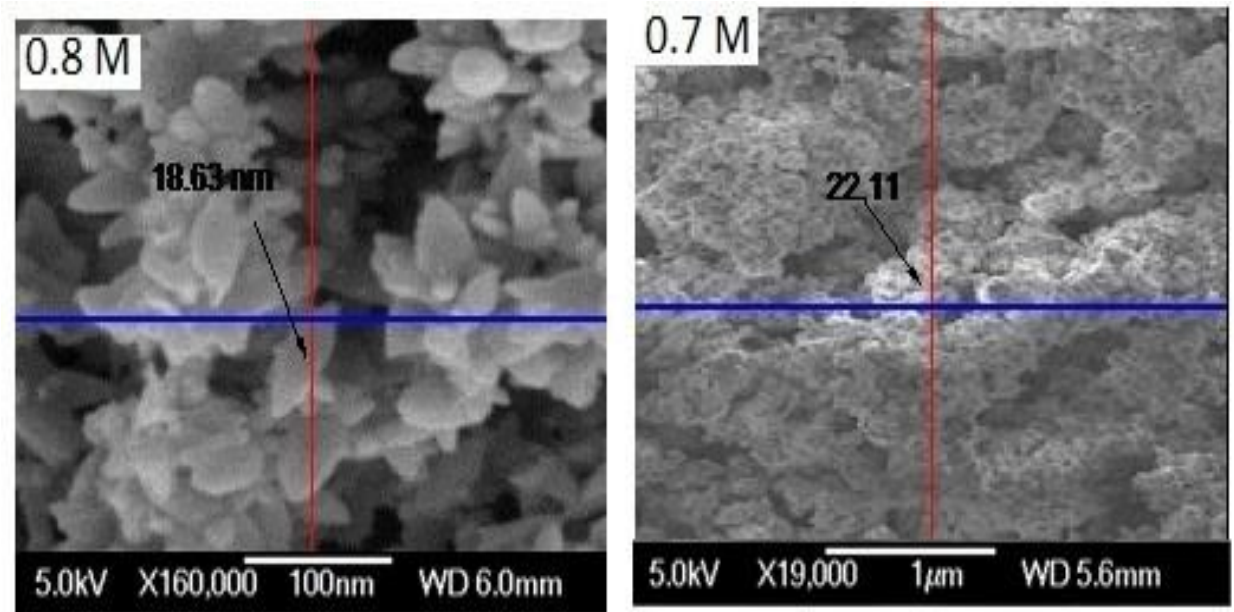


Figure (4.17): shows the SEM images for samples 0.8 M and 0.7M respectively

The SEM image of sample ZnO 0.6 M nanostructures are shown in Fig (4.18). The morphology in Figure (4.18, 0.6 M) indicates the as-synthesized of ZnO 0.6 M presents like-date nanostructures. The like-datenanostructures of synthesized ZnO (0.6 mol) are agglomerated together in uniform shape. The mean particle size was estimated from SEM is equal to 68.47 nm in well agreement with size calculated from XRD data 68.47 nm. Figure (4.18, 0.5 M) shows low magnification image of ZnO 0.5 M film nanostructures using zinc acetate of concentration 0.5 mol. It can be easily observed that the nanostructures are aligned and closely crammed together in a large quantity with uniform surface. The average size of these like-datenanostructures was approximated from the SEM image and found to be 92.15 nm comparing to average size of 92.15 nm of ZnO 0.5 M are in a good agreement with the size obtaining from XRD data table (4.2).

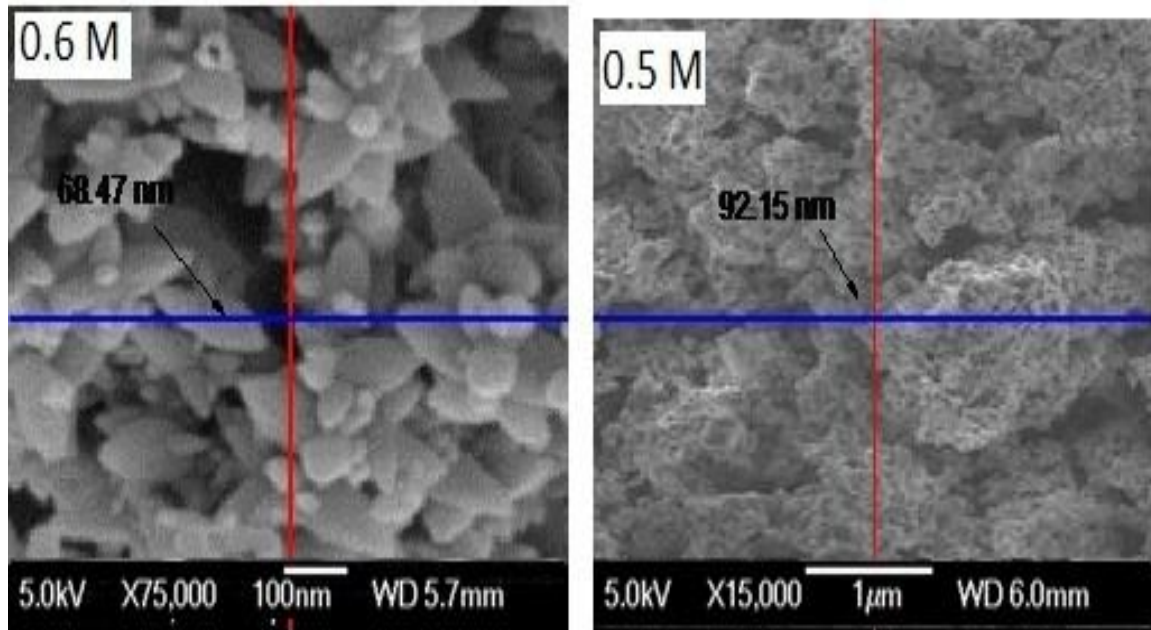


Figure (4.18): shows the SEM images for samples 0.6 M and 0.5 M respectively

The SEM image of sample ZnO 0.4 M nanostructures are shown in Fig (4.19). The SEM image is clearly confirmed that the synthesized ZnO 0.4 M materials are pointed to nanostructures forms that grown in a large quantity. Interestingly, it is seen that the pointed nanostructures are assembled in bunches and each bunch containing a large amount of nanostructures. This nanostructures of synthesized ZnO (0.4 mol) are agglomerated together in uniform shape. The mean particle size was estimated from SEM is equal to 108.00 nm which close to that calculated from XRD data. Figure (4.19, 0.3 M) shows a low magnification image of ZnO 0.3 M sample using zinc acetate of concentration 0.3 mol. It can be purely seen that the nanostructures are aligned and gathering together in a large amount with uniform surface. The average size of these nanostructures was estimated from the SEM graph and found to be 114.83 nm comparing to average size of 114.83 nm of ZnO 0.3 M sample calculated using the XRD data table (4.2).

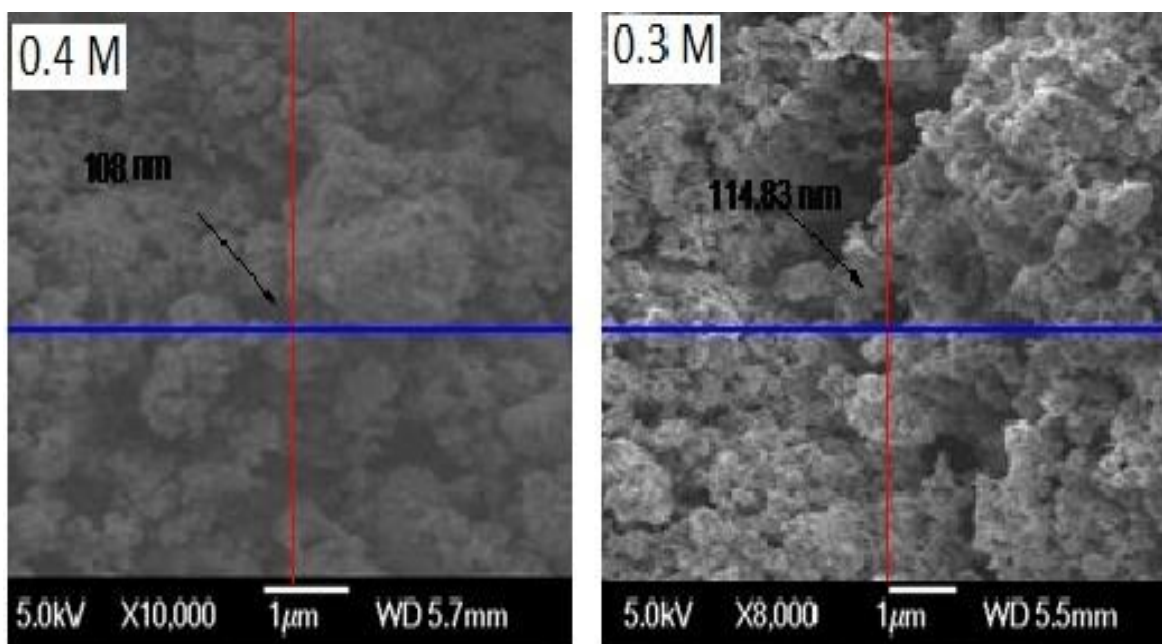
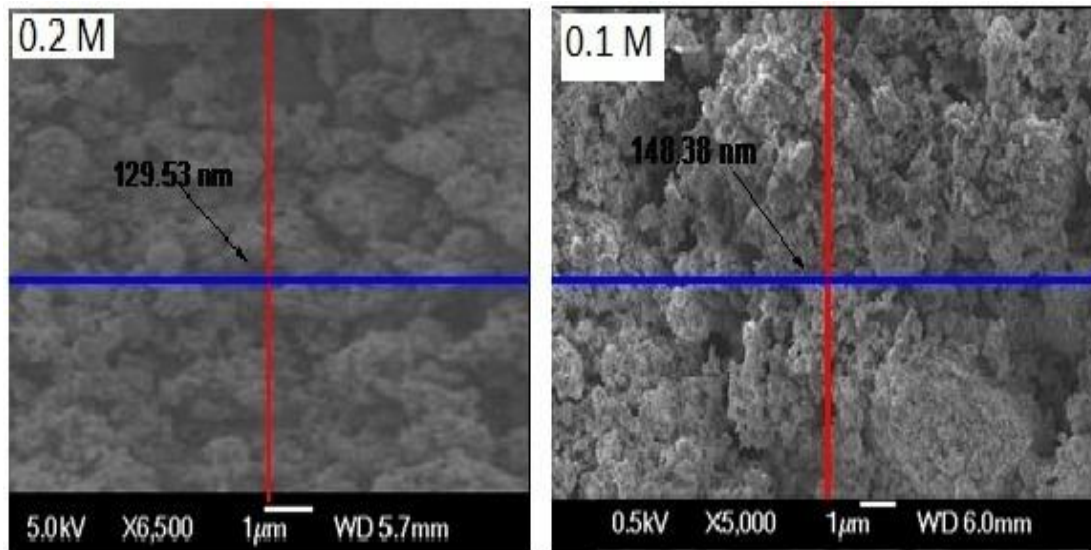


Figure (4.19): shows the SEM images for samples 0.4 M and 0.3 M respectively.

The as-synthesized products of sample ZnO 0.2 M is characterized by SEM and the micrograph are reported in Figure (4.20.0.2 M).The SEM image is clearly confirm that the synthesized ZnO 0.2 M materials containing nanostructures that grown in large quantities. Interestingly, it is seen that the as-obtained nanocomposie/nanoparticlesfor sample ZnO 0.2 M are assembled in bunches and each bunch containing a large amount of nanostructures. This nanostructures of synthesized ZnO (0.2 mol) are agglomerated together in uniform shape. The mean particle size was estimated from SEM is equal to 129.53 nm, much agree with size calculated from XRD data 129.53nm. Figure (4.20, 0.1M) shows low magnification image of ZnO 0.1 M sample using zinc acetate of concentration of 0.1mol. Also, it can be easily seen that the nanostrutures are gathering together in a large amountwith uniform surface. The average size of these nanostructures was estimated from the SEM graph and found to be 148.38 nm comparing to average size of 145.23 nm of ZnO 0.1 M in a good agreement with size calculated using the XRD data table (4.2).

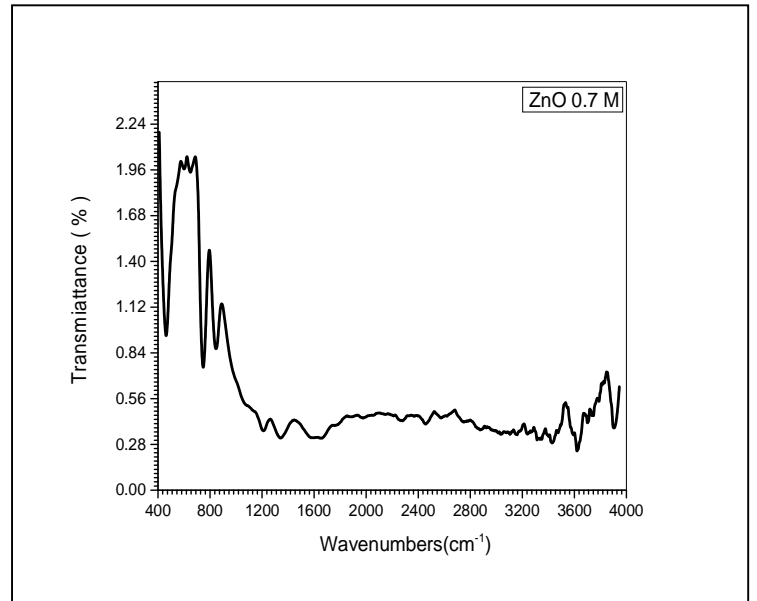
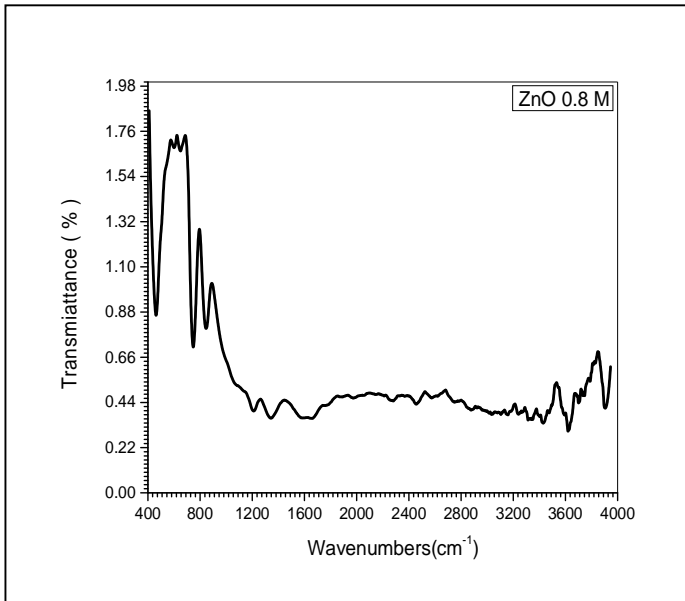
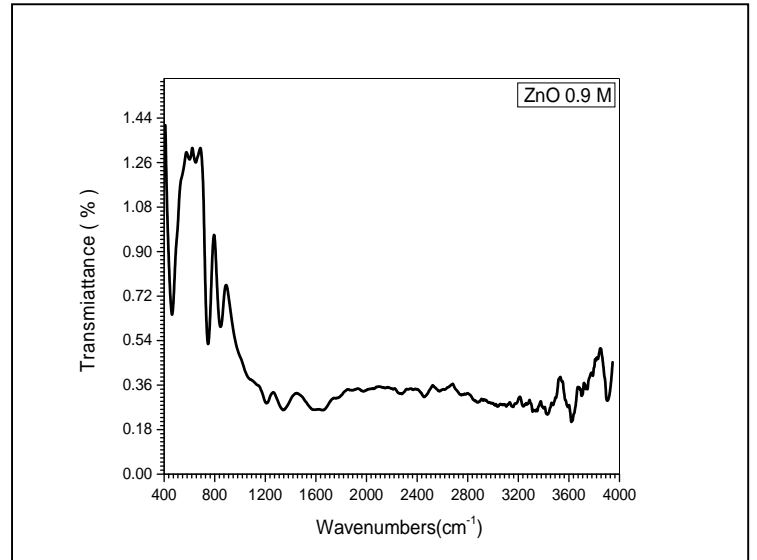
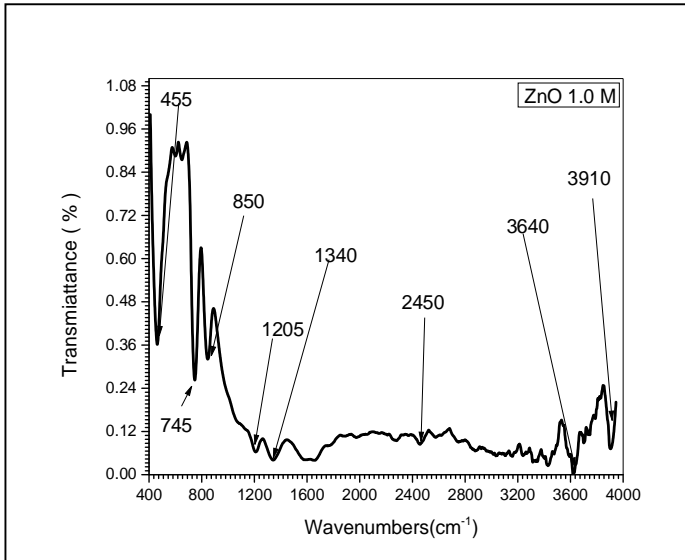


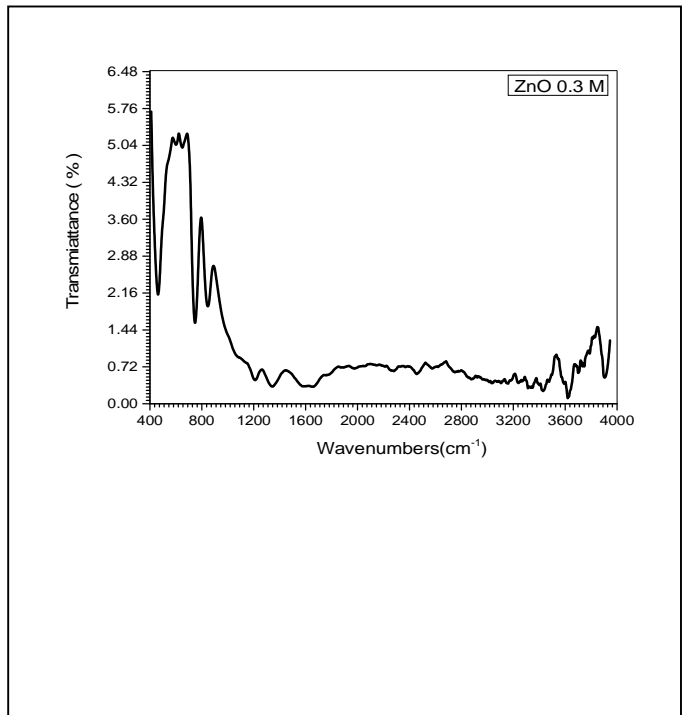
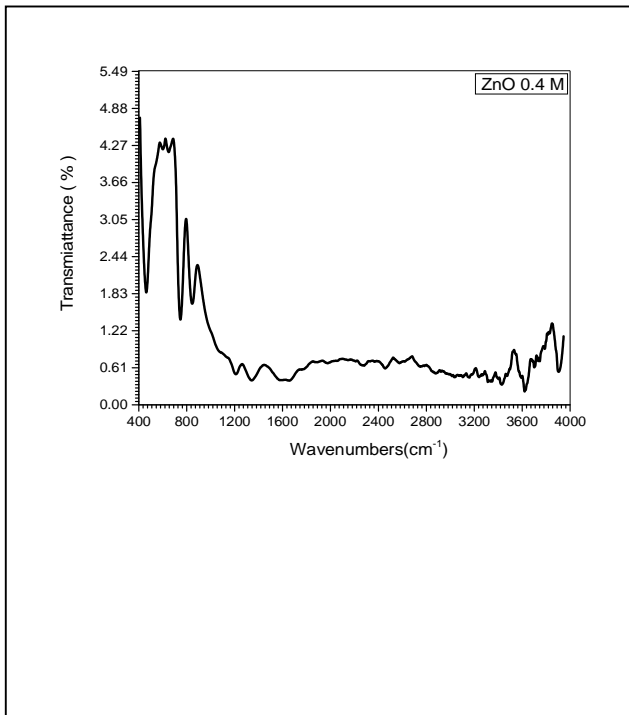
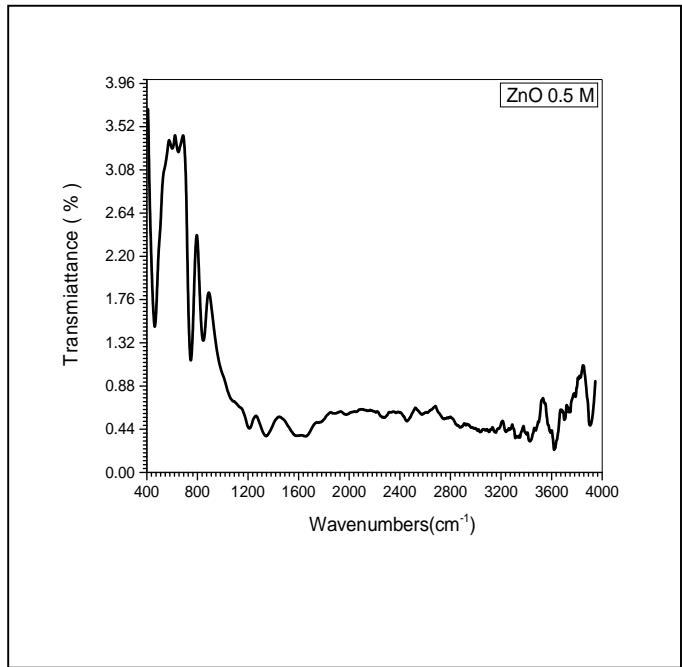
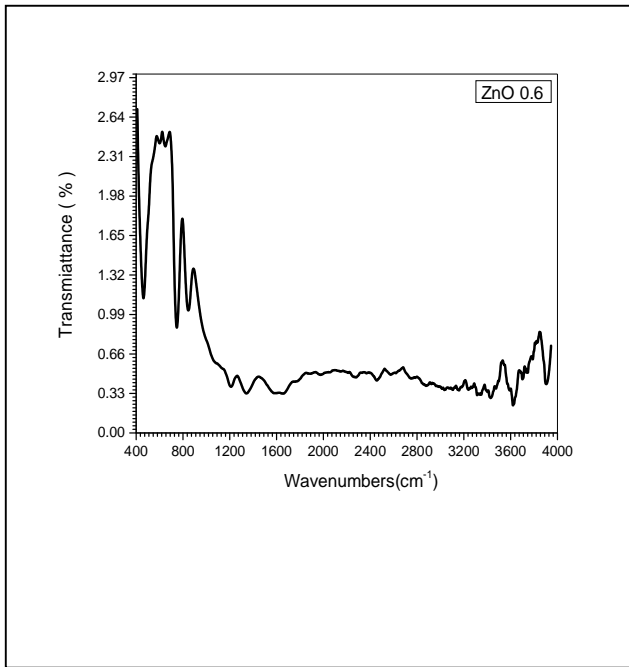
Figure(4.20): shows the SEM images for samples 0.2 M and 0.1M respectively

4.4 Fourier Transform Infrared Spectrophotometer (FTIR) analysis

The infrared spectra of the ten samples of synthesized ZnO films nanostructures using different concentrations of zinc acetate were recorded by mattson Fourier Transform Infrared Spectrophotometer in the range of 400 to 4000 cm^{-1} (Figures 4.21 from 1.0 M to 0.1 M). The spectra of FTIR resulted that all of as-synthesized ZnO samples indicated some locations of the band positions, Table 4.3. In the present study the absorption bands are denoted as ν_1 , ν_2 , ν_3 , ν_4 , ν_5 , ν_6 , ν_7 and ν_8 as shown in table 4.3. These absorption bands are found to be around 455 cm^{-1} , 745 cm^{-1} , 850 cm^{-1} , 1205 cm^{-1} , 1340 cm^{-1} , 2450 cm^{-1} , 3640 cm^{-1} and 3910 cm^{-1} respectively for all the samples synthesized in this study. The transmittance bands within these specific limits revealed the formation of single-phase spinel structure having two sub-lattices tetrahedral (A) site and octahedral (B) site. The band around $455 - 850\text{ cm}^{-1}$ is caused by the metal-oxygen vibration in the tetrahedral side. This difference in the spectral positions is due to the different of distance values of metal ion- O^{2-} for octahedral and tetrahedral sites. The band around 1205 is due to C-C stretching mode and C-C-H bending vibration. The band around 1340 cm^{-1} is associated with the O-H bending vibration. The band around 2450 cm^{-1} is due to C=C stretching mode. The location of the absorption bands at the

positions ν_7 and ν_8 are around 3640cm^{-1} and 3910cm^{-1} , is due to the stretching mode of H-O-H bending vibration of free charge or absorbed water which implies that the hydroxyl groups are retained in ZnO for different concentrations [92, 93].





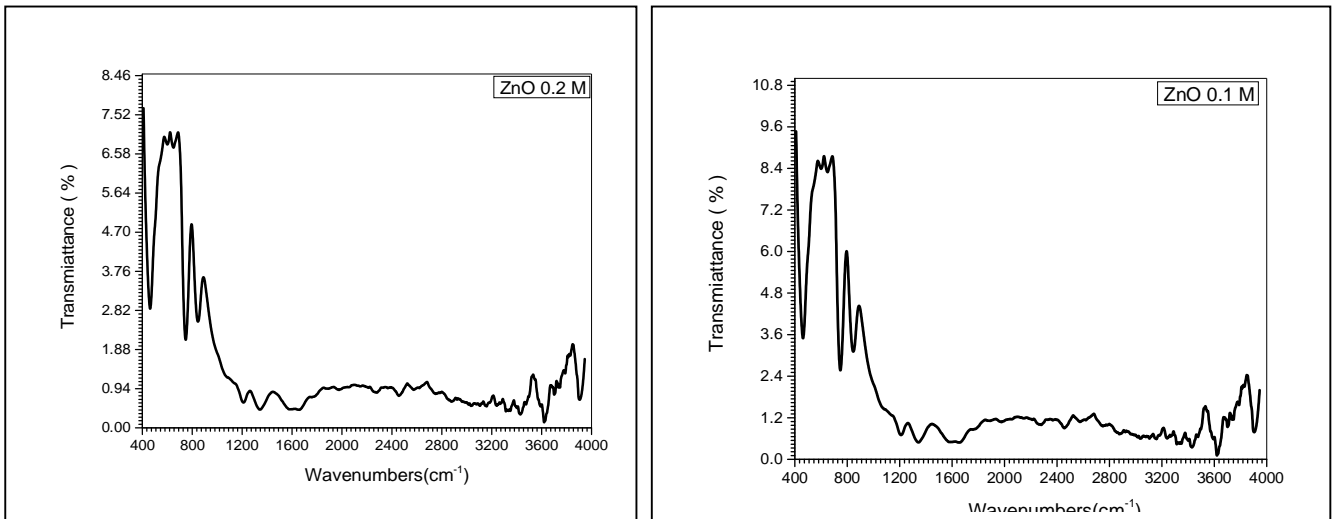


Figure (4.21) : represents the FTIR spectrums of as-synthesized ZnO nanostructures for the ten samples symbolized in molar form 1.0 M to 0.1 M respectively.

The FTIR spectrums for all samples of synthesized ZnO/films nanostructures are combined together as shown in Figure (4:22). The results concluded that all samples have same or sharing the exact absorption bands around 455cm^{-1} , 745cm^{-1} , 850cm^{-1} , 1205cm^{-1} , 1340cm^{-1} , 2450cm^{-1} , 3640cm^{-1} and 3910cm^{-1} respectively. The sharp peaks appeared at 455cm^{-1} and 745cm^{-1} are related with metal-oxygen (Zn-O) bond and confirms that the synthesized material is ZnO nanostructures [94, 95]. As general the presence of well-defined Zn-O band in the FTIR spectrum confirmed that the prepared nanostructures are pure ZnO without any significant impurity.

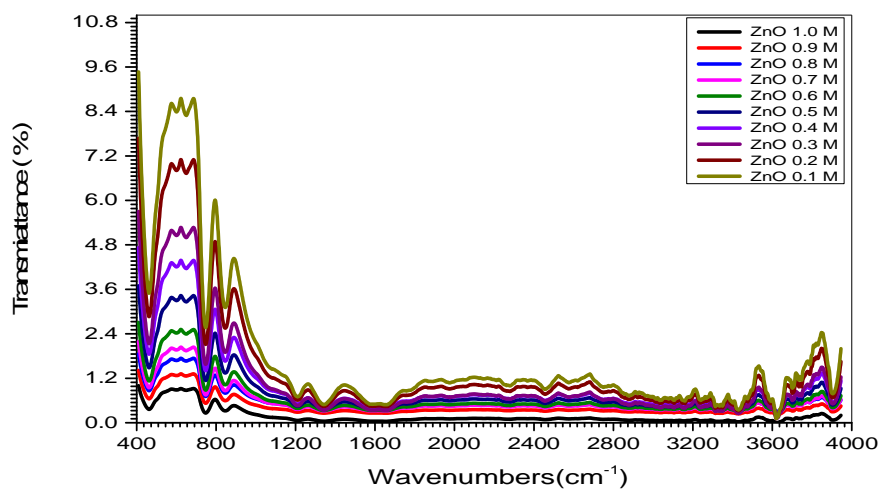


Figure (4:22):FTIR spectrum of the ten samples of as-synthesis ZnO film nanostructures.

Table 4.3: FTIR Parameters in (cm^{-1}) of the ten samples of synthesized ZnO nanostructures using different concentration of zinc acetate.

| Compounds | ν_1 | ν_2 | ν_3 | ν_4 | ν_5 | ν_6 | ν_7 | ν_8 |
|-----------|---------|---------|---------|---------|---------|---------|---------|---------|
| ZnO 0.1 M | 455 | 745 | 850 | 1205 | 1340 | 2450 | 3640 | 3910 |
| ZnO 0.2 M | 455 | 745 | 850 | 1205 | 1340 | 2450 | 3640 | 3910 |
| ZnO 0.3 M | 455 | 745 | 850 | 1205 | 1340 | 2450 | 3640 | 3910 |
| ZnO 0.4 M | 455 | 745 | 850 | 1205 | 1340 | 2450 | 3640 | 3910 |
| ZnO 0.5M | 455 | 745 | 850 | 1205 | 1340 | 2450 | 3640 | 3910 |
| ZnO 0.6 M | 455 | 745 | 850 | 1205 | 1340 | 2450 | 3640 | 3910 |
| ZnO 0.7 M | 455 | 745 | 850 | 1205 | 1340 | 2450 | 3640 | 3910 |
| ZnO 0.8 M | 455 | 745 | 850 | 1205 | 1340 | 2450 | 3640 | 3910 |
| ZnO 0.9 M | 455 | 745 | 850 | 1205 | 1340 | 2450 | 3640 | 3910 |
| ZnO 1.0 M | 455 | 745 | 850 | 1205 | 1340 | 2450 | 3640 | 3910 |

4.5 The Optical Properties of ZnO Nanostructures

To evaluate the optical properties, the as-synthesized ZnO film nanostructures were examined by using UV-visible (UV-Vis) min 1240 spectrophotometer after dispersion in water by means of ultrasounds at room-temperature. These optical properties are:

4.5.1 The Absorbance

Figure (4.23) illustrates the typical UV-Vis spectrum of as-synthesized ZnO nanostructures and well-defined the absorbance characteristic of the ten samples synthesizing by using different concentrations of zinc acetate with amounts of 1.0 ,0.9, 0.8 ,0.7 ,0.6 ,0.5 ,0.4 ,0.3 ,0.2 and 0.1 molars respectively. As can be noticed, the absorbance spectrum for all samples of as-synthesised ZnO thin films nanostructures shows one broad absorbance band at 275 nm and this may attributed to the reduction in crystallite size of the cubic structure[96]. Moreover, Figure (4.23) indicates that the absorbance characteristic of ZnO thin films nanostructures are gradually increase when increasing the concentrations of zinc acetate. This is since, by adding more zinc acetate

may help the as-synthesised ZnO thin films nanostructures to absorb the incident radiation by its free electrons.

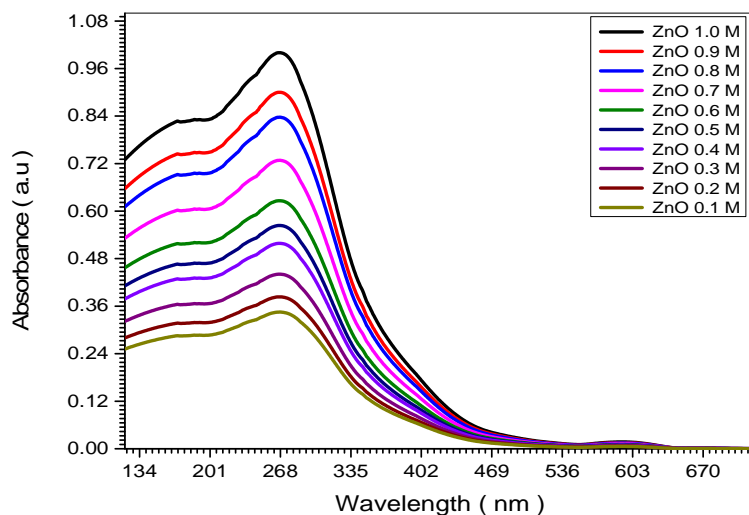
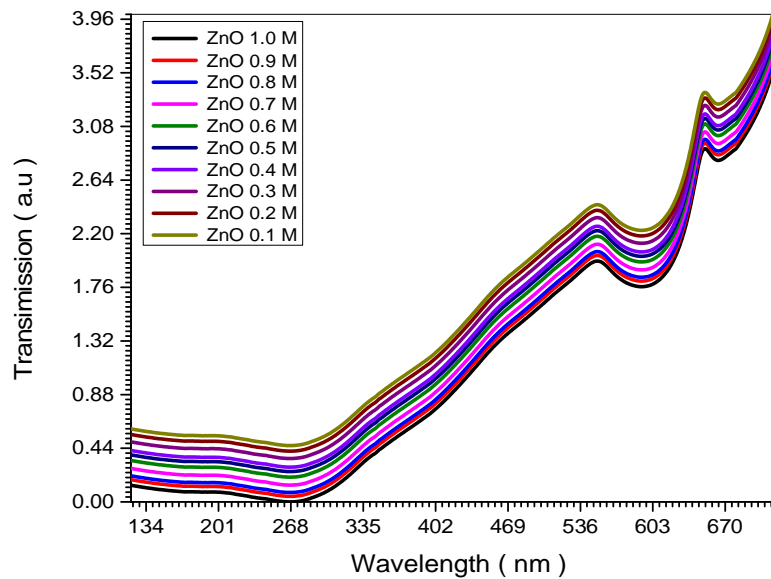


Figure (4.23): shows the relation between absorbance and wavelengths of the ten samples of as-synthesised ZnO thin film nanostructures.

4.5.2 The Transmittance

The transmittance spectrum of the ten samples of the synthesized ZnO nanostructures were investigated via UV-visible spectroscopy in the range of 120 - 720 nm. Figure (4.24) designed the relation between the transmittance and the wavelengths of the ten samples of as-synthesised ZnO films nanostructures. Under the condition of different concentrations of zinc acetate, the results showed that all of as-synthesized samples of ZnO nanostructures can reach a saturation before wavelength of 276 nm and the average transmittance value of the samples equal 1.495 a.u. Figure (4.24) also shows that the transmittance values decreased with increasing the concentrations of zinc acetate.



Figure(4.24): Indicates the relation between transimission and wavelenghts of the ten samples of as-synthesised ZnO thin film nanostructures.

4.5.3 The Reflectance

Figure (4.25) shows the reflectance spectrum of the ten samples of as-synthesised ZnO nanostructures at different concentrations of zinc acetate. Thereflectance spectrum expanded from 134 to 415 nm. Figure (4.25) shows that the reflectance can be shifted to blue region at a particular wavelenghts of 415.4 nm, 410 nm and 406 nm for samples 1.0 M, 0.9 M and 0.8 M respectively. Also the Figure(4.25) represents that at low concentration of zinc acetate0.1M the reflection is shifted to 348.4 nm in the region of ultravilot. Therefor, the result concluded that the reflectance spectrum in this study are restricted in the range of 348.4 nm to 415.4 nm.

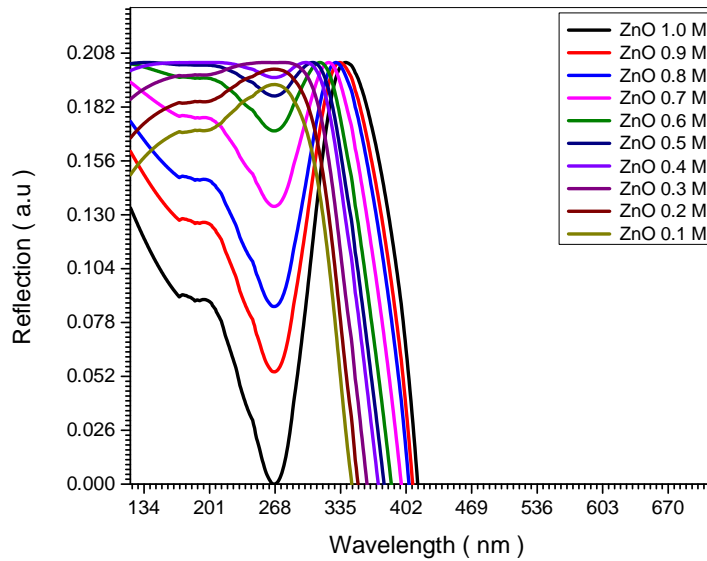


Figure (4.25): shows the relation between reflection and wavelengths of Ten samples of as-synthesized ZnO film nanostructures.

4.5.4 Absorption Coefficient

The absorption coefficient (α) of as-synthesized ZnO films nanostructures reported in this study can be obtained by using Beer-Lambert's relation:

$$\alpha = \frac{2.303xA}{t} \quad (4.2)$$

where (A) is the absorbance and (t) is the thickness of the film. Figure (4.26) shows a plotting graph between the absorption coefficient (α) and the wavelength (λ) of ten samples of the synthesized ZnO nanostructures. The results indicate that the maximum value of α is $4.63 \times 10^3 \text{ cm}^{-1}$ materialized in the U.V region at the peak of wavelength 270 nm corresponding the concentration of 1.0 molar of zinc acetate where the absorption coefficient at same wavelength decreases to $\alpha = 1.34 \times 10^3 \text{ cm}^{-1}$ for low concentration of 0.1 molar of zinc acetate. High value of α means that the transition must match to direct electronic transition, and the properties of this state are important since they are responsible for electrical conduction.

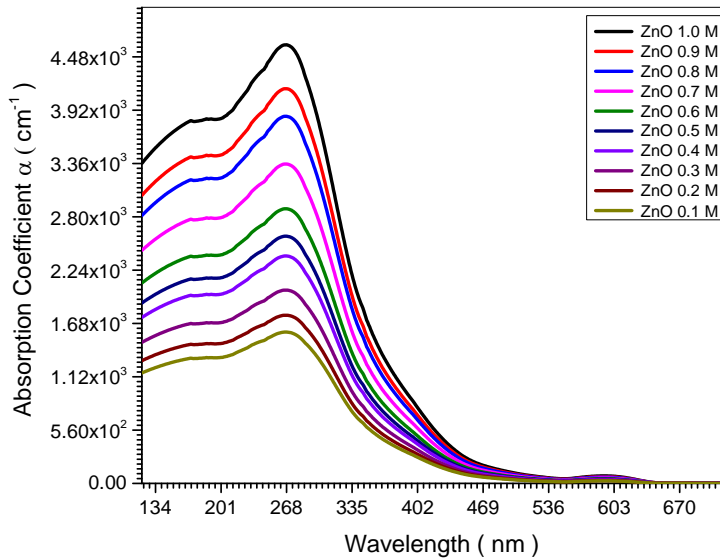


Figure (4.26): shows the relation between the absorption coefficient and the wavelengths of ten samples of as-synthesized ZnO films nanostructures.

4.5.5 Extinction Coefficient (K)

Extinction coefficient (K) was calculated using the relation:

$$k = \frac{\alpha\lambda}{4\pi} \quad (4.3)$$

Where α is absorption coefficient and λ is the wavelength. Figure(4.27) shows the values of the extinction coefficient (K) as a function of wavelength (λ) for the ten samples of synthesized ZnO nanostructure using different molarities of zinc acetate. It is observed that the shape of the extinction coefficient spectrum is similar to the shape of the absorption coefficient (α) Figure (4.26). The values of extinction coefficient K for the ten samples of synthesized ZnO films nanostructures were measured at the range (120 - 720 nm). As can be seen, the value of (K) at the maximum peak of wavelength 277 nm is 1.0084×10^{-2} for high concentration (ZnO 1.0 Molar) while for low concentration (ZnO 0.1 Molar) at the same wavelength is equal to 3.44×10^{-3} . As a result, the values of the extinction

coefficient (K) increased with increasing the molar concentrations of zinc acetate during synthesizing the ZnO film nanostructures.

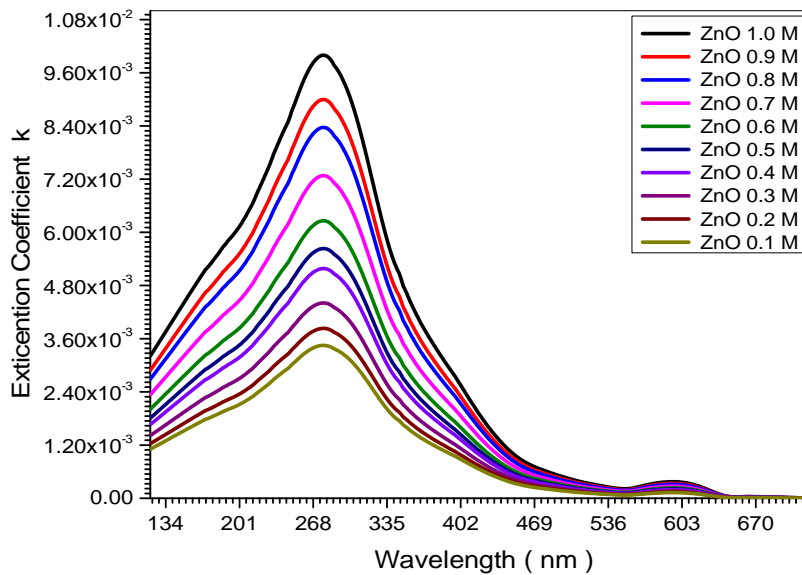


Figure (4.27): shows the relation between the extinction coefficient and wavelengths of ten samples of as-synthesized ZnO films nanostructures.

4.5.6 The Refractive Index (n)

The refractive index (n) plays a very important role in optical communication and the most desirable optical constants of photonic materials for the fabrication of quantum photonic devices. The refractive index (n) can be calculated by using the following relation:

$$n = \left[\left(\frac{1+R}{1-R} \right)^2 - (1 + k^2) \right]^{\frac{1}{2}} + \frac{(1+R)}{(1-R)} \quad (4.4)$$

where (R) is the reflectivity and k is the extinction coefficient where $k = \frac{\alpha\lambda}{4\pi}$. Figure (4.28) shows the refractive index (n) of as-synthesized ZnO films nanostructures as a function of wavelength. Figure (4.28) confirmed that at the range of 422 - 469 nm all the curves of the refractive index (n) of the as-synthesized samples represented a maximum peak at $n = 2.159$, except samples 0.2 M and 0.1 M showed refractive index values of 2.128 and 2.044 respectively. This result nearly agrees with the standard refractive index $n = 2.004$ of ZnO [97, 98]. Also, the result demonstrated that the value of (n) begins to

decrease between the wavelengths 306 - 344 nm at the region of the spectrum. This behavior may due to the nature of the sharp absorption of Zinc Oxide nanostructures that lead to an electronic transmission at the absorption edge.

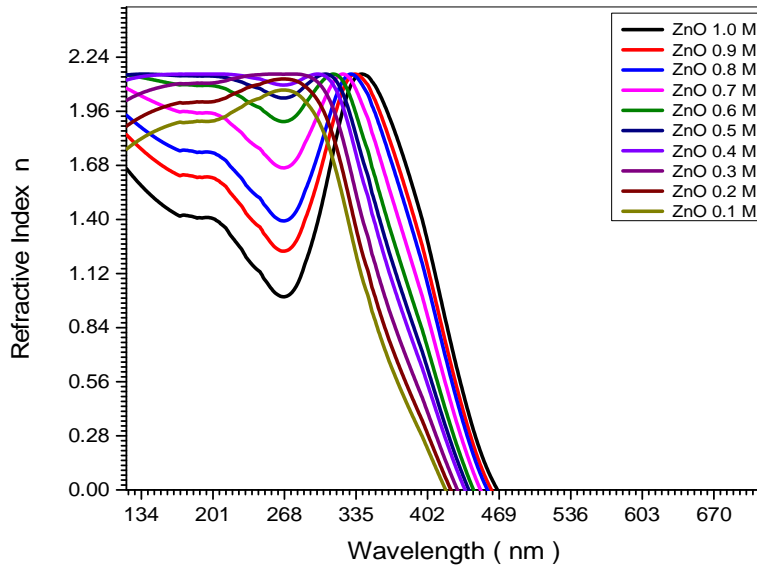


Figure (4.28):represents the refractive index of the ten samples of as-synthesised ZnO nanostructures as function of wavelength.

4.5.7 The Optical Energy Gap (E_g):

The optical energy gap E_g has been calculated by using the following relation:

$$(\alpha h\nu)^2 = C(h\nu - E_g) \quad (4.5)$$

where α is the absorption coefficient , C is constant and E_g is the bandgap energy. The direct bandgap energies were determined for the different concentrations of zinc acetate of as-synthesised ZnO thin films nanostructures by plotting $(\alpha h\nu)^2$ versus photon energy ($h\nu$) as shown in Figure (4.29). The optical bandgap values are obtained from the graph $(\alpha h\nu)^2$ vs. $h\nu$ by extrapolating the linear portion of the plot to $(\alpha h\nu)^2=0$, Figure(4.29). The results indicated that the ZnO film nanostructures that synthesized by using 0.1 molar of zinc acetate has the highest value of bandgap (3.889) eV, whereas those synthesized by using 1.0 molar

exhibited the lowest value bandgap (3.443 eV), which believed to possess a better conductivity [99]. The result indicated that for the less concentrations 0.1, 0.2, 0.3, 0.4 and 0.5 molar, large values of the optical bandgap energies can be obtained, which means there are more electrons that adopt more energy levels located in the bottom of the conduction band. As can be observed, the bandgap energy decreases with increasing concentration of the zinc acetate dehydrate. This decrease could be due to stress relaxation in the film and the smallest size of as-obtained like-date nanostructures [100]. Also the bandgap energy of the as-synthesized ZnO nanostructures showed a red-shift from 0.16 eV (for 1.0 molar) to 0.28 eV (for 0.1 molar) comparing to the bandgap of bulk ZnO of 3.6 eV [101]. This shifting can be attributed to quantum confinement effect of the formation of ZnO nanostructures.

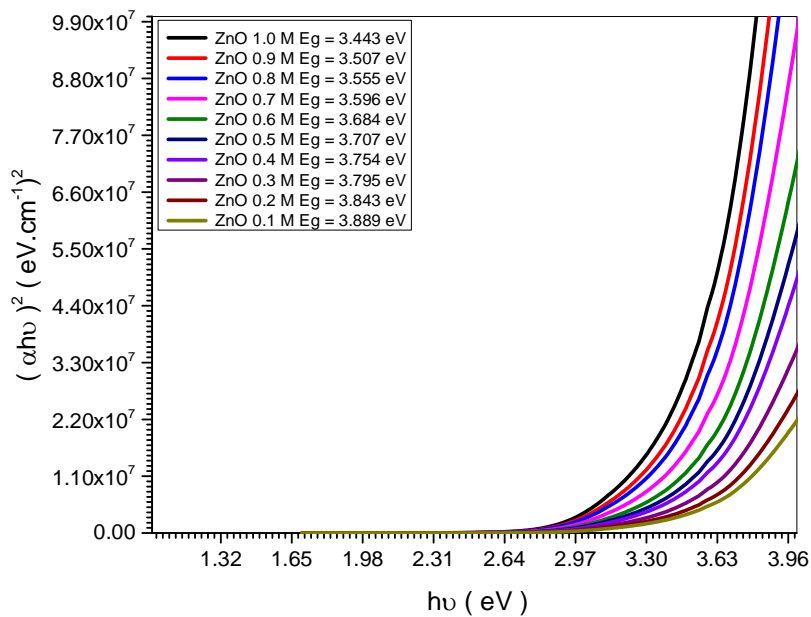


Figure (4.29): Plot of $(\alpha h\nu)^2$ versus the photon energy ($h\nu$) for ZnO nanostructures synthesized by using different concentrations of zinc acetate.

4.5.8 Real Dielectric Constant (ϵ_1):

Figure (4.30) shows the real dielectric constant (ϵ_1) of the ten samples of synthesized ZnO nanostructures versus the wavelength. The real dielectric constant (ϵ_1) was calculated using the relation :

$$\epsilon_1 = n^2 - k^2 \quad (4.6)$$

Where k is extinction coefficient and n is the refractive index. The real dielectric (ϵ_1) is the normal dielectric constant. Figure (4.30) indicated that the variation of (ϵ_1) pattern is follow the same pattern of refractive index Figure (4.28), this means that the refractive index was dominated in this behavior. Also, from Figure (4.30) the value of the real dielectric constant (ϵ_1) for the sample at higher concentrations (ZnO 1.0 M) is equal to 4.617 at the broad peak of wavelength 344 nm whereas for the sample ZnO 0.1M of lower concentration is found to be 4.026 at the broad peak of wavelength 281 nm. As general, the pattern of the real dielectric constant (ϵ_1) in this study is clearly blue-shift when increasing the concentration of zinc acetate.

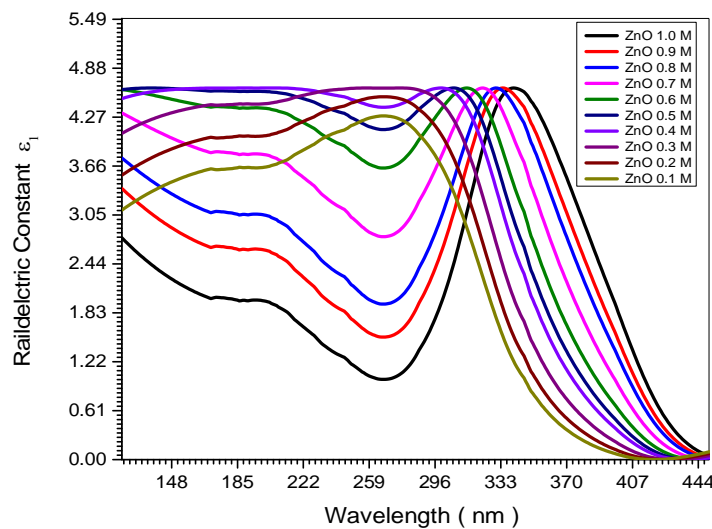


Figure (4.30): shows the relation between the real dielectric constant and the wavelengths of the ten samples of as-synthesized ZnO films nanostructures.

4.5.9 Imaginary Dielectric Constant (ϵ_2)

The imaginary dielectric constant (ϵ_2) versus the wavelength (λ) was shown in Figure(4.31). The values ϵ_2 have been calculated by using the relation:

$$\epsilon_2 = 2nk \quad (4.7)$$

Where k is extinction coefficient and n is the refractive index. The imaginary dielectric constant (ϵ_2) represents the absorption associated with free carriers. The value of ϵ_2 at maximum peak of sample (1.0 M) is equal 2.84×10^{-2} at the broad peak of wavelength 323 nm whereas, for sample ZnO 0.1M is found to be 1.33×10^{-2} at the broad peak of the wavelength 273 nm. Interestingly, although the samples 0.1 M , 0.2 M, 0.3 M, 0.4 M and 0.5 M sharing the same broad peak of the wavelength 273 nm showed different values of imaginary dielectric constant. As general, the results of the imaginary dielectric constant patterns showed that the values of ϵ_2 are decreasing with decreasing the concentration of zinc acetate during synthesizing ZnO film nanostructures. The disparity in values of ϵ_1 and ϵ_2 may be attributed to the different in absorption mechanism for free carriers

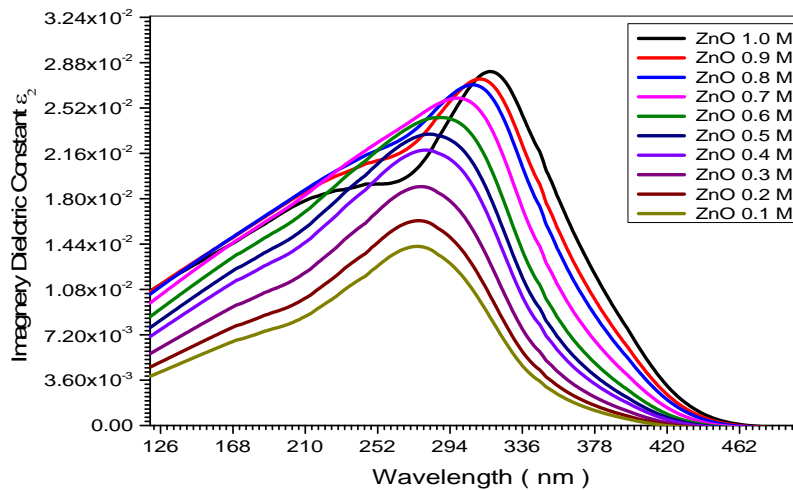


Figure (4.31): The relation between imaginary dielectric constant and wavelengths of the ten samples of as-synthesized ZnO film nanostructures.

4.5.10 The Optical and The Electrical Conductivity

The optical conductivity is a measure of frequency response of material when irradiated with light, and can be determined by using the following relation [99]:

$$\delta_{opt} = \frac{\alpha nc}{4\pi} \quad (4.8)$$

Where (c) is the light velocity, δ_{opt} is optical conductivity, n is refractive index and α is the absorption coefficient. The electrical conductivity can be estimated using the following relation :

$$\delta_{ele} = \frac{2\lambda\delta_{opt}}{\alpha} \quad (4.9)$$

Where λ is the wavelength. The high magnitude of optical conductivity is about $1.34 \times 10^{11} \text{ sec}^{-1}$ observed in Figure(4.32) which confirms the presence of very high photo-response for samples 1.0 M, 0.9 M, 0.8 M and 0.7 M respectively of as-prepared ZnO nanostructures. The increase of optical conductivity at high concentrations is due to the high absorbance of as-prepared samples ZnO and also may attributed to electron excitation by photon energy. In addition, samples 0.1 M, 0.2 M, 0.3 M, 0.4 M, 0.5 M and 0.6 M representing same broad peak at wavelength of 268 nm with optical conductivities of $7.48 \times 10^{10} \text{ sec}^{-1}$, $9.01 \times 10^{10} \text{ sec}^{-1}$, $1.04 \times 10^{11} \text{ sec}^{-1}$, $1.17 \times 10^{11} \text{ sec}^{-1}$, $1.258 \times 10^{11} \text{ sec}^{-1}$ and $1.309 \times 10^{11} \text{ sec}^{-1}$ respectively. Moreover, Figure (4.27) indicates that electrical conductivity is equal to $32.5 (\Omega \text{ cm})^{-1}$ for sample 1.0 M of high concentrations while equal to $27.42 (\Omega \text{ cm})^{-1}$ for sample 0.1 M of low concentration. As a results, the electrical conductivity increases with increasing the concentrations of zinc acetate and that means the high concentration could account as an optimal condition for large electrical conductivity. Moreover, decreasing the concentrations during synthesizing the ZnO film/ITO glass causes a reduction in the film's electric conductivity [99, 101] which lead to increasing in resistivity.

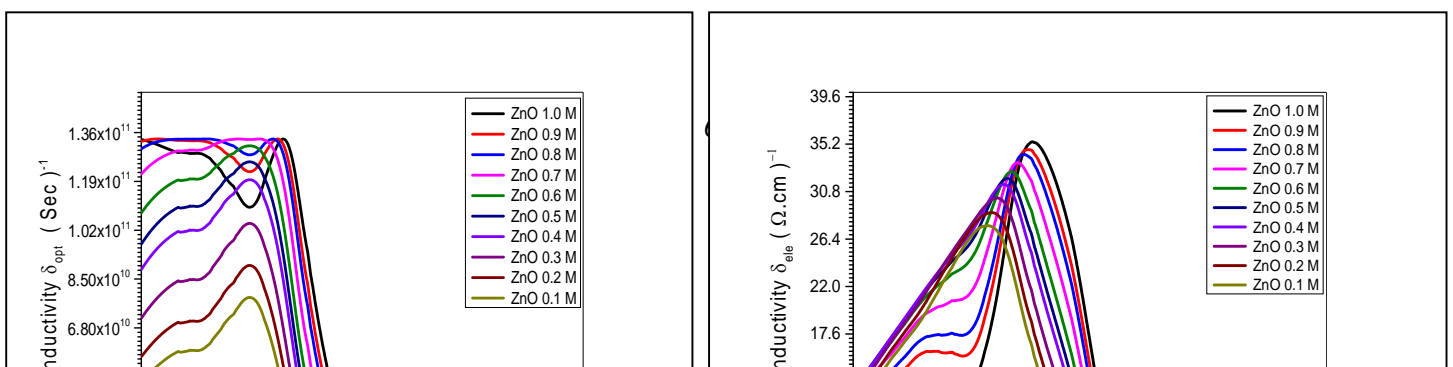


Figure (4.32): Shows the relation between, (a) the optical conductivity and (b) electrical conductivity versus the wavelengths of ten samples of as-synthesized ZnO nanostructures.

Chapter Five

Conclusion and Recommendations

This chapter presented the main works done in this thesis and proposes some future works. In conclusion, we have successfully synthesized ZnO films nanostructures through sol-gel method by using different concentrations of zinc acetate arranged as 1.0, 0.9, 0.8, 0.7, 0.6, 0.5, 0.4, 0.3, 0.2 and 0.1 molars respectively. The structural, the morphological and the optical properties have been carried out for all samples of as-synthesized ZnO nanostructures.

The results from XRD demonstrated that all samples show local cubic of ZnO structure with unit cell parameter $a = 0.8398$ nm. Among the extensive experiments, the result assured that the concentration of 1.0 mol of zinc acetate should be the best amount to promote the crystallite control and the best for reducing particles size to 20.10 nm comparing with the rest molars of zinc acetate used in this study. Also the results from Fourier Transform Infrared Spectrometer (FTIR) spectrum confirmed the location of the absorption bands at the positions around 3640cm^{-1} and 3910cm^{-1} , are due to the stretching mode of H-O-H bending vibration of free charge or absorbed water which implies that the hydroxyl groups are retained in ZnO for different concentrations.

The top-view SEM images of as-synthesized ZnO nanostructures for all samples have been studied by using the Scanning Electron Microscopy (SEM). The detailed morphological studies revealed that the synthesized ZnO material possessed like-rod shaped of intermingled nanostructures. The size of the particle like-nanorods were decreasing with increasing the concentrations of zinc acetate that means the difference in the concentrations may play a role to decrease the size of nanostructures. As a result, sample 1.0M made nanostructures like-rod of ZnO with average size of 11.77 nm while for sample 0.1M made nanostructures with size of 148.38 nm. The sizes of the nanostructure for sample 1.0 M showed 20.1 nm from XRD data while for SEM equal to 11.77 nm, and this may be attributed to that the size of nanostructure represented in SEM image was taken from a region containing nanoparticles have different sizes that differ from the other regions.

Concerning, the optical properties of as-synthesized ZnO film nanostructures: the study confirmed that the absorbance spectrum for all samples of as-synthesized ZnO thin films

nanostructures showed a broad band at 275 nm, and this may attributed to the reduction in crystallite size of the cubic structure. Also the absorbance exhibited that, adding more zinc acetate lead to the as-synthesised ZnO thin films nanostructures to absorb the incident radiation by its free electrons. The study revealed that the average transmittance value of the samples equal to 1.495 a.u. In addition the results confirmed that the transmittion values decreased with increasing the concentrations of zinc acetate. Interestingly, the reflectance can be shifted to blue region at a particular wavelengths of 415.4 nm, 410 nm and 406 nm for samples 1.0 M, 0.9 M and 0.8 M while at low concentration of zinc acetate 0.1M the refelection was shifted to 348.4 nm.

The absorption coefficient (α) at the peak of wavelength 270 nm are found to be $4.63 \times 10^3 \text{ cm}^{-1}$ as maximum value for sample 1.0 moalr, where it equal $1.34 \times 10^3 \text{ cm}^{-1}$ at same wavelength for sample 0.1 M. Moreover, the values of the extinction coefficient (K) in this study are increased with increasing the molar concentrations of zinc acetae during synthesising the ZnO film nanostructures. This study exposeed that the refractive index (n) of as-synthesized ZnO nanostructures are ranged between $n = 2.159$ to $n = 2.044$ in good agreement with standard value of 2.004. Interstingly, the thesis established that the ZnO film nanostructures has the highest value of bandgap energy 3.889 eV for sample 0.1 molar of zinc acetate , whereas it exhibited the lowest value bandgap of 3.443 eV for sample 1.0 molar which believed to possess a better coductivty. Also, the resultshows that large values of the opical bandgap can be obtaiend for concentrations 0.1. 0.2, 0.3, 0.4 and 0.5 molars, and this may help more electrons can adopt more energy levels located in thebottom of the conduction band.

The values of the real dielectric constant (ϵ_1) of the sample (ZnO 1.0 M) at higher concentration is equal to 4.617 and for sample 0.1 M at low concentration is equal to 2.84×10^{-2} , which is clearly confirmed blue-shift when incresingthe concentration of zinc acetate. Finally, the optical and the electrical conductivities have been obtained and the results established that the high magnitude of optical conductivity is about $1.34 \times 10^{11} \text{ sec}^{-1}$ for samples 1.0 M, 0.9 M and 0.8 M molars which confirms the presence of very high photo-response for these samples. Also, the study showed the magnitude of electrical

conductivity for sample 1.0 M is equal to $32.5 (\Omega \text{ cm})^{-1}$ and for sample 0.1 M equal to $27.42 (\Omega \text{ cm})^{-1}$.

Generally, it is concluded that the presented thesis has explored the effect of the concentrations of zinc acetate on the successful synthesis, the characterization and the physical properties of ZnO films nanostructures, prepared by simple techniques, sol- gel process. The detailed compositional, structural and optical properties confirmed that the synthesized material was pure ZnO and possessed well-crystalline local cubic phase and exhibited good optical properties. Therefore, it is my personal belief that this study opens a way for future works that simply synthesized ZnO nanomaterials can efficiently be used for the fabrication of high-efficient dye-sensitized solar cell applications and can be used as efficient electron mediators for the fabrication of various effective chemical sensors. Finally, I hope that the work presented in this thesis has contributed in some or other way in the synthesis, characterization and physical properties of some ZnO films nanostructures.

References

- [1]. C. N. R. Rao, A. Muller, A. K. Cheetham, The Chemistry of Nanomaterials: Synthesis, Properties and Applications Willey, Weinheim (2004).
- [2]. A. K. Bandyopadhyay, Nano Materials: in Architecture, Interior Architecture and Design, New Age International, New Delhi (2008).
- [3]. J. D. Meindl, Q. Chen and J. A. Davis, Science 293 (2001) 2044.

- [4]. C. M. Leiber, *Sci. Am.* 58 (2001).
- [5]. P. Yang, *MRS Bull.* 30 (2005) 85.
- [6]. D.C. Coffey and D. S. Ginger, *Nature Materials* 5 (2006) 735.
- [7]. M. Muccini, *Nature Materials* 5 (2006) 605.
- [8]. K. Nomura, H. Ohta, A. Takagi, T. Kamiya, M. Hirano and H. Hosono, *Nature* 432 (2004) 488.
- [9]. J. L. G. Fierro, *Metal Oxides: Chemistry and Applications*, CRC Press, Florida (2006).
- [10]. V. E. Henrich, P. A. Cox, *The Surface Chemistry of Metal Oxides*, Cambridge University Press, Cambridge, UK (1994).
- [11]. C. Noguera, *Physics and Chemistry at Oxide Surfaces*, Cambridge University Press, Cambridge, UK (1996).
- [12]. A. R. José, F.-G. Marcos, *Synthesis, Properties, and Applications of Oxide Nanomaterials*, Willey, New Jersey (2007).
- [13] Sara Marouf^a, Abdelkrim Beniaiche^a, Hocine Guessas^a, Amor Azizi^b, *Materials Research* DOI: <http://dx.doi.org/10.1590/1980-5373-MR-2015-0751>
- [14] Khalaf Al Abdullah, Sahar AWAD, Jean Zaraket and Chafic Salame, *Energy Procedia* 119 (2017) 565- 570.
- [15]S. Jurablu, M. Farahmandjou*, and T. P. Firoozabadi, *Journal of Sciences, Islamic Republic of Iran* 26 (2015)281 – 285.
- [16] Bevan D.J.M. and Anderson J.S., *Discussions of the Faraday Society*, 8 (1950) 238-246.
- [17] Cooley A.J., London: R. Hardwicke. 1866 p. 812.
- [18] Harrison S.E., *Physical Review*, 93(1954) 52-62.
- [19] Dudkowsk S., Kepka A.G., and Grosswei L., *Journal of Physics and Chemistry of Solids*, 28(1967) 485-493.
- [20] Henglein A., *Berichte Der Bunsen-Gesellschaft-Physical Chemistry Chemical Physics*, 101(1997) 1562-1572.
- [21] Dong L.F., Cui Z.L., and Zhang Z.K., *Nanostructured Materials*, 8(1997) 815-823.
- [22] Huang M.H., Mao S., Feick H., Yan H., Wu Y., Kind H., Weber E., Russo R., and Yang P., *Science*, 292(2001) 1897-1899.
- [23] Pearton S.J., Abernathy C.R., Overberg M.E., Thaler G.T., Norton D.P., Theodoropoulou N., Hebard A.F., Park Y.D., Ren F., Kim J., and Boatner L.A., *Journal of Applied Physics*, 93(2003) 1-13.
- [24] Ozgur U., Alivov Y.I., Liu C., Teke A., Reshchikov M.A., Dogan S., Avrutin V., Cho S.J., and Morkoc H., *Journal of Applied Physics*, 98(2005).
- [25] Klingshirn C., *ChemPhysChem*, 8(2007) 782-803.
- [26]. F.K.III. Urban, A. Hosseini-Tehrani, P. Griffiths, A. Khabari, Y.W. Kim, Petrov I. *J Vac. Sci. Technol. B* 20 (2002) 995.
- [27]. T. Karabacak, A. Mallikarjunan, et al., . *Appl. Phys. Lett.* 83 (2003) 3096.
- [28]. L.M Cao, Z. Zhang et al., *Adv. Mater.* 13 (2001) 1701.
- [29]. L.M. Cao, K. Hahn et al., *Appl. Phys. Lett.* 80 (2002) 4226.
- [30]. A.P. Weber, M. Seipenbusch, G. Kasper, *J. Phys. Chem. A* 105 (2001) 8958.
- [31]. E.F. Rexer, D.B. Wilbur, J.L. Mills, R.L. DeLeon, J.F. Garvey. *Rev. Sci. Instrum.* 71 (2000) 2125.
- [32]. C.J. Brinker, G.W. Scherer, *Sol-Gel Science*, Academic Press, Inc.: New York, (1990).
- [33]. L.L. Hench, J.K. West, *Chem. Rev. (Washington, D.C.)*, 90 (1990) 33.
- [34]. B. O'Regan, J. Moser, M. Anderson, M. Graetzel, *J. Phys. Chem.* 94 (1990) 8720.
- [35]. R. Kaur, A.V. Singh et al., *J. Non-Cryst. Solids*, 32 (2006) 2565.
- [36]. Y.W. Chen, Y.C. Liu, et al., *J. Chem. Phys.* 123 (2005) 134701.
- [37]. X.Y. Wang, X.Y. Wang, et al., *J. Power Sources* 140 (2005) 211.
- [38]. H. Xu, D.H. Qin, Z. Yang, H.L. Li, *Mater. Chem. Phys.* 80 (2003) 524.

- [39]. Ozgur U., Alivov Y.I., Liu C., Teke A., Reshchikov M.A., Dogan S., Avrutin V., Cho S.J., and Morkoc H., *Journal of Applied Physics*, 98(2005).
- [40]. Akira O. and Masaki T., *Electronic Ferroelectricity in II-VI Semiconductor ZnO*. 2012.
- [41]. X.Y. Wang, X.Y. Wang, et al., *J. Power Sources* 140 (2005) 211.
- [42]. H. Xu, D.H. Qin, Z. Yang, H.L. Li, *Mater. Chem. Phys.* 80 (2003) 524.
- [43]. M. Zhang, Y. Bando and K. Wada, *J. Mater. Sci. Lett.* 20 (2001) 167.
- [44]. J.H. Yang, G.M. Liu, L. Jun, Y.F. Qiu, S.H. Yang, *Appl. Phys. Lett.* 90 (2007) 103109.
- [45]. C.S. Rout, S.H. Krishna, et al., *Chem. Phys. Lett.* 418 (2006) 586.
- [46] Regional Sophisticated Instrumentation Centre PU, Chd, Retrieved on May 4,2010 from: <http://rsic.puchd.ac.in/em.html>.
- [47] What is SEM? Iowa State Varsity, MME dept., Retrieved on May 4, 2010 from:<http://mse.iastate.edu/microscopy/whatsem.html>
- [48] Sato, H., Minami, T., Takata, S., Mouri, T., Ogawa, N. *Thin Solid Films*, Vol. 220 (1992), pp. 327 and Vol. 246 (1994), pp. 86.
- [49] Zinc oxide applications, Retrieved on May 4, 2010 from:<http://www.stallonezincoxide.com/application.htm>
- [50] Zinc oxide (ZnO) Properties and Applications, Retrieved on May 4, 2010 from <http://www.azom.com/details.asp?ArticleID=2357>
- [51] Zinc oxide applications, Retrieved on May 4, 2010 from:<http://www.ucalanka.com/zinc-oxide-applications.html>
- [52] Zinc oxide application, Retrieved on May 4, 2010 from:<http://www.numinor.com/application.asp>
- [53] Zinc oxide applications, Retrieved on May 4, 2010 from:http://wapedia.mobi/en/Zinc_oxide?.
- [54] Hagfeldt A., Boschloo G., Sun L., Kloo L., and Pettersson H., *Chemical Reviews*, 110(2010) 6595-6663.
- [55]. Keis K., Magnusson E., Lindström H., Lindquist S.-E., and Hagfeldt A., *Solar Energy Materials and Solar Cells*, 73(2002) 51-58.
- [56] Ko S.H., Lee D., Kang H.W., Nam K.H., Yeo J.Y., Hong S.J., Grigoropoulos C.P., and Sung H.J., *Nano Letters*, 11(2011) 666-671.
- [57]. T.T. Kang, X. Liu, R.Q. Zhang, W.G. Hu, G. Cong, F.Zhao and Q. Zhu, *Appl. Phys. Lett.* 89 (2006) 71-113
- [58]. J.B. Baxter, E.S. Aydil, *Appl. Phys. Lett.* 86 (2005) 53.
- [59] Omaneh J, *Novel Synthesis Techniques for Nanostructures: Doctoral thesis*, P.2 (2004).
- [60]HF.Hussein,chufran, *Jmatter. Environ.sci.* 2(2011)426.
- [61] Kim, K. *Journal of the Korean Physical Society*, 55 (2009) 140.
- [62] Jiang J, Wang L, Yang Q & Yang D, *Journal of Inorganic Materials*, 21 (2006) 833.
- [63]. W. I. Park, D. H. Kim, S.-W. Jung, and G.C. Yi, *Appl. Phys. Lett.* 80 (2002) 4232.
- [64]. B.P. Zhang, N.T. Binh, Y. Segawa, K. Wakatsuki and N. Usami, *Appl. Phys. Lett.* 83 (2003) 1635.
- [65]. W. Lee, H.G. Sohn and J.M. Myoung, *Mater. Sci. Forum* 449 (2004) 1245.
- [66]. J. Su, M. Gherasimova, et al., *Appl. Phys. Lett.* 87 (2005) 183108
- [67]. J.B. Baxter, E.S. Aydil, *Appl. Phys. Lett.* 86 (2005) 053114.
- [68] . B. Djuričić, X. Y. Chen and Y. H. Lung, *Recent Pat. Nanotechnol*, 6(2012)124.
- [69] D. Chen, X. Ciao and G. Cheng, *Solid State Commun.*, 2000, 113, 363.
- [70] A. A. Ismail, A. El-Midany, E. A. Abdel-Aal and H. El-Shall, *Mater. Lett.*, 2005, 59, 1924.
- [71] S. Musić, D. Dragčević, S. Popović and M. Ivanda, *Mater. Lett.*, 59 (2005) 2388.
- [72] S. J. Chen, L. H. Li, X. T. Chen, Z. Xue, J. M. Hong and X. Z. You, *J. Cryst. Growth*, 252(2003)184.
- [73] J. Zhang, J. Wang, S. Zhou, K. Duan, B. Feng, J. Weng, H. Tang and P. Wu, *J. Mater. Chem*, 20 (2010) 9798.
- [74] J. Ma, J. Liu, Y. Bao, Z. Zhu, X. Wang and J. Zhang, *Ceram. Int.*, 39 (2013) 2803.

- [75] . Kołodziejczak-Radzimska, T. Jesionowski and A. Krysztalkiewicz, *Physicochem. Probl. Miner. Process.*, 44 (2010) 93.
- [76] R. Hong, T. Pan, J. Qian and H. Li, *Chem. Eng. J.*, 119 (2006) 71.
- [77] W. Jia, S. Dang, H. Liu, Z. Zhang, C. Yu, X. Liu and B. Xu, *Mater. Lett.*, 82 (2012) 99.
- [78] Selma M. H. Al-Jawad¹, Sabah H. Sabeeh¹, Hussein A. Jassim¹, Natheer Jamal Imran². *Iraqi Journal of Physics*, 17(2019) 95-107.
- [79] Kai Loong Foo, Uda Hashim, Kashif Muhammad and Chun Hong Voon, *Nanoscale Research Letters*, 9 (2014) 429.
- [80] H.F. Hussein¹, Ghufran Mohammad Shabeeb², S.Sh. Hashim, *J. Mater. Environ. Sci.* 2 (2011) 423-426.
- [81] Basics of X Ray Diffraction, Scintag Inc., 1999, Chapter 7, pp. 7.13-7.14.
- [82] Single Crystal X-ray Diffraction, Christine M. Clark, Eastern Michigan University, Barbara L. Dutrow, Louisiana State University, Retrieved April 22 2010 from http://serc.carleton.edu/research_education/geochemsheets/techniques/SXD.html
- [83]. mmrc.caltech.edu/FTIR/FTIRintro.pdf
- [84]. http://en.wikipedia.org/wiki/Fourier_transform_infrared_spectroscopy#Conceptual_introduction.
- [85] Michael D & Adaskaveg J E, *Introduction to the Scanning Electron Microscope*, book, (1997).
- [86] Egerton & Ray, *Physical Principles of Electron Microscopy*, book, 2005.
- [87] Kim, S.-K., Jeong, S.-Y. and Cho, C.-R. (2003) *Applied Physics Letters*, 82, 562.
- [88] Wang, Zhong Lin, *J. Phys.: Condens. Matter*. Vol. 16 (2004), pp. R829–R858.
- [89] Ü. Özgür, Ya. I. Alivov, C. Liu, A. Teke, M. A. Reshchikov, S. Doğan, V. Avrutin, S.-J. Cho, and H. Morkoç, *Journal of applied physics*. Vol. 98 (2005), pp. 041301.
- [90] *Zinc Oxide: Fundamentals, Materials and Device Technology*. Copyright _ 2009 WILEY-VCH Verlag GmbH & Co. KGaA, Weinheim ISBN: 978-3-527-40813-9
- [91] Cullity B D 1956 *Elements of X-Ray Diffraction* (Reading, MA: Addison-Wesley) Appendix 1 (A1-1) p 459.
- [92]. A.P. Alivisatos, *J. Phys. Chem.* 100(13) (1996) 226.
- [93]. C. Burda, X. Chen, R. Narayanan, M.A. El-Sayed, *Chem. Rev.* 105 (2005) 1025.
- [94]. W. H. Zhang, and J. S. Zhao, *Journal of Molecular Structure* 789 (2006) 177.
- [95]. S.Y. Bae, H.W. Seo and J.H. Park, *J. Phys. Chem. B* 108 (2004) 5206,
- [96] F. Decremps,^{a)} J. Pellicer-Porres,^{b)} F. Datchi, J. P. Itié^{c)}, A. Polian, and F. Baudelet, *APPLIED PHYSICS LETTERS*, 18 (2002) 4820-482
- [97] Y. Li, G.S. Tompa, S. Liang, C. Gorla, C. Lu, J. Doyle, *J Vac Sci Technol A* 15(1997) 1663.
- [98] D.W. Palmer, Available from: <http://www.semiconductors.co.uk>, 2002.06.
- [99]. A.F. Mansour, S.F. Monsour and M.A. Abdo, *Improvement Structural and Optical Properties of ZnO/PVA nanocomposites*, 2015, 11: 60-69.
- [100] Bhavana N. Joshi, Hyun Yoon, Ho Young Kim, Joon Ho Oh, Tae Yeon Seong, Scott. James, and Sam S. Yoon, *Journal of The Electrochemical Society*, 159 ((2012) H716-H721
- [101]. R. Menon, K. Sreenivas, and V. Gupta, *J. Appl. Phys.*, 103, 094903 (2008)

Appendix: publishing papers arising out of this thesis

1) ¹A. B. Awatif*, ²Mubarak Dirar Abdallah, ³Abdalsakhi S M.H, ⁴E.M. Elssfah
⁵Aldesogi Omer Hamed, ⁶Rawia Abd Elgani Elobaid, **Effect of Different Concentrations of Zinc Acetate on the Structural, and the Optical and**

Electrical Conductivity of ZnO Nanostructures, IOSR Journal of Applied Physics (IOSR-JAP) e-ISSN: 2278-4861. Volume 11, Issue 6 Ser. I (Nov. – Dec. 2019), PP 35-40.

2) A. B. Awatif, ²Mubarak Dirar Abdallah, ³E.M. Elssfah ⁴ Abdalsakhi S M.H,
Optical Properties of ZnO Nanostructures Synthesised Using Different Concentrations of Zinc Acetate, IOSR Journal Of Applied Physics (IOSR-JAP) e-ISSN: 2278-4861. Volume 12, Issue 2 Ser. I (Mar. – Apr. 2020), PP 01-06.